# EXPLORING CYTOPLASMIC DYNEIN AND α, β-TUBULIN HETERODIMER INTERACTIONS: INSIGHTS FROM MOLECULAR DYNAMICS SIMULATIONS ON NEURONAL FUNCTION AND DISEASE

BY

NISARG DAVE

A Thesis submitted to the Psychology Department

In partial fulfillment of the Requirements for the Honours

Degree, Faculty of Science

Department of Psychology

Memorial University of Newfoundland and Labrador

Honours 499B

August 2023

**Abstract**

Intracellular motor protein dynein, known for its role in cellular transport, interacts intimately with α, β-tubulin heterodimers of microtubules (MTs). Using an all-atom Molecular Dynamics (MD) simulation technique, the nuanced dynamics of dynein's Microtubule Binding Domain (MTBD) and the association with the tubulin heterodimer subunit were investigated. The significance of tubulins' C-terminal tails (CTTs) and their distinct fluctuations are highlighted, revealing their contribution to dynein's structural stability and conformational changes. Further, the investigation delves into the conformational changes across the α-H14-B10 loop, α-H14, and β-H7, elucidating their high RMSF values and critical role in binding interactions. The complex interplay of distance relationships between MTBD and tubulin subunit further reinforces these protein interactions' dynamic nature. Findings also revealed key insights into salt bridge interactions and potential electrostatic forces. The study is aimed to explore the MTBD's structural dynamics, advancing understanding of dynein function and setting the stage for future therapeutic research targeting this motor protein.

*This research is a qualitative analysis based on a 320 ns length trajectory. Given the inherent time constraints, the simulations performed for this study did not progress to convergence and the later stages of the simulation.*

**Acknowledgement**

I want to express my profound gratitude to my advisors, Dr. Alisaraie and Dr. Walling. Their unending support, encouragement, and guidance have been instrumental in completing this thesis. Their expertise and meticulous attention to detail have significantly shaped my understanding and approach to the subject matter. I appreciate their invaluable advice, constant encouragement, and constructive critiques. Further, my gratitude extends to Jivesh Garg for his vital assistance in lab work and Compute Alliance Canada for their indispensable technological support.

I must also extend my most profound appreciation to my loving mother and godfather. Their unyielding support and unwavering faith in me have been the backbone of my academic journey. They have always believed in my capabilities and aspirations, standing by me through the ups and downs. Their strength and resilience have motivated me to persevere in my studies.

Thank you to my family and friends for their love, encouragement, and understanding. Their constant support and belief in me have been invaluable. They have stood by me through late nights and early mornings. The motivation, inspiration, and laughter they brought into my life made the journey bearable and enjoyable.

**Table of Contents**

Page

Abstract ..... i

Acknowledgement ..... ii

Table of Contents ..... iii

List of Figures ..... v

1. Introduction ..... 1

1.1 Dynein's Role in Disease Modeling ..... 2

1.2 Structural Components and Motility of Dynein ..... 3

1.3 Importance and Dynamics of Microtubules ..... 8

1.4 Studying Biological Systems Through Molecular Dynamics Simulations ..... 12

2. Methods ..... 14

3. Results ..... 16

3.1 RMSD Analysis of System Components ..... 22

3.2 RMSF Analysis of System Components ..... 29

3.3 dCOM Analysis of Potential Interactions between System Components ..... 32

3.4 Salt Bridge Analysis of System Components ..... 41

4. Discussion ..... 43

4.1 RMSD of System Components ..... 43

4.2 RMSF of System Components ..... 44

4.3 dCOM Analysis and Potential Interactions between System Components ..... 45

4.4 Salt Bridge Analysis ..... 48

5. Conclusion ..... 51

6. References ..... 53

## List of Figures

Page

**Figure 1**. *Cytoplasmic Dynein Motor Domain with αβ-Tubulin Dimer, Highlighting Stalk, α-Helices, MTBD, and Colored AAA+ ATPase Modules* ……..……...….5

**Figure 2.** *Stages and Conformational Changes in Dynein Motility*.....7

**Figure 3**. *Microtubules and the seven PTMs of CTTs* ……..…….....9

**Figure 4.** *Initial Configuration of the Dynein-Tubulin System Highlighting Key Components and Interaction Complexity*.....18

**Figure 5.** *Color-Coded Representation of Dynein's MTBD Helices* ……..….... 19

**Figure 6** *Superimposed Structures of the Initial and Final System States Following Simulation*……..…….....20

**Figure 7** *Comparative Analysis of MTBD Helical Shifts: Superimposed Structures at 0 ns and 319.5 ns Simulation Timepoints Fluctuations*.....21

**Figure 8.** RMSD of the Complete system including CTTs and Dyenin Stalk ……..... 23

**Figure 9** *RMSD of the Complete system including CTTs and Dyenin Stalk* …….24

**Figure 10** *RMSD of α-tubulin*.....25

**Figure 11** *RMSD of β-tubulin* .....26

**Figure12** *RMSD of α-CTT* ….....27

**Figure 13 .** *RMSD of β-CTT*... .....28

**Figure 14** *RMSF of Heterodimer throughout 319 ns* .....30

**Figure15.** *Root-Mean-Square Fluctuation of Microtubule-Binding Domain Residues*…….....31

**Figure 16 .** *dCOM Analysis of Interactions Between Tubulins* …….....34

**Figure17.***dCOM Analysis Between Tubulin CTTs and MTBD*….....35

**Figure 18 .** *dCOM Analysis Between Tubulin CTTs and MTBD-H7*…….....36

**Figure 19** *dCOM Analysis Between Tubulin CTTs and MTBD-H3* ……..37

**Figure 20** d*COM Analysis Between Tubulin and MTBD-H5* …….. 38

**Figure 21** d*COM Analysis Between Tubulin and MTBD-H3*…… 39

**Figure 22** d*COM Analysis Between Tubulin and MTBD-H1*…… 40

**Figure 23 .** *Structural Insight into Dynein MTBD-Tubulin Interaction via Salt Bridges*……..42

# Exploring Cytoplasmic Dynein and αβ-Tubulin Heterodimer Interactions: Insights from Molecular Dynamics Simulations on Neuronal Function and Disease

## 1. Introduction

Motor proteins are fundamental biological molecules, performing critical mechanical tasks within cells by harnessing energy from adenosine triphosphate (ATP) hydrolysis (Howard, 1997; Vale, 2003). One of these motor proteins, cytoplasmic dynein, plays a crucial role in various neuronal processes, including intracellular, axonal, and dendritic transport (Moughamian & Holzbaur, 2018). Dynin facilitates these processes by transporting cargo along microtubules (MTs), cylindrical, hollow cytoskeleton protofilaments composed of α-, β-tubulin heterodimers (Moughamian & Holzbaur, 2018). These MTs feature C-terminal tubulin tails (CTTs), which are variable and unstructured regions with several functions, such as maintaining MT stability and interacting with other proteins (Janke & Magiera, 2020). Past research suggests that these CTTs play an interactive role with motor proteins such as dynein, facilitating not only the binding to the main body of microtubules but also influencing dynein motility (Ayloo et al., 2017; Bodakuntla et al., 2021; Ferro et al., 2020; Heale & Alisaraie, 2020; Uchimura et al., 2015). In this thesis, an all-atom MD simulation technique was employed to examine the interactions of the MTBD-stalk with α and β tubulin heterodimer to analyze the motion, motility, and changes in the conformation of dynein. It is hypothesized that changes in the structure, conformations, and motility mechanism of dynein is partly due to binding interactions of CTTs.

### 1.1 Dynein's Role in Disease Modeling

The dynein family comprises two functional classes, axonemal and cytoplasmic (Burgess et al., 2003; Höök & Vallee, 2006; Vale, 2003). Amidst these diverse isoforms cytoplasmic, dynein-I performs retrograde transport along MTs (Höök & Vallee, 2006; Schmidt & Carter, 2016). Neuronal cells can reach up to a meter in length, making long-distance retrograde transport of celluar cargo and organic materials essential for maintenance and mechanical functionality (Moughamian & Holzbaur, 2018). Cytoplasmic dynein performs both dendritic and slow axonal transport in neuronal cells. Dynein is especially important for transporting cargo with high molecular weights greater than 2 Da, as they are incapable of moving autonomously within the cytoplasm (Reck-Peterson et al., 2018). Dynein's transport in dendrites is regulated through polarized targeting into and out of dendritic compartments (Bodakuntla et al., 2021). Dynein has a significant contribution to the trafficking of neurotrophic signals, such as Neurotropic Growth Factor (NGF) and Brain-Derived Neurotrophic Factor (BDNF) from the terminal axon region to the nucleus, triggering changes in gene expression (Hirokawa et al., 2010). Neurotrophic factors and their signalling are essential in triggering neuronal growth (Kowiański et al., 2018).

During cortical development, dynein has a vital function in neuronal migration, through which neuronal nuclei move from their origin to their final location in the cortex (Wynshaw-Boris, 2007). Mutations in dynein disrupt function associated with neuronal migration, thus resulting in cortical malformations like lissencephaly, a condition denoted by a smooth brain surface and diminished cortical folds (Aiken et al., 2019; Markus et al., 2020; Wynshaw-Boris, 2007). Huntingtin, a protein implicated in the progression of

Huntington's disease, aggregates within neurons, causing neurodegeneration (Zuccato et al., 2010). Interestingly dynein and huntingtin have colocalized with Tropomyosin receptor kinase B (TrkB) and BDNF in dendrites. Early indicators of the ALS disease process are associated with impairments in rapid axonal transport, displayed in both *in vitro* and *in vivo* models (Marinković et al., 2012; Perlson et al., 2009).

The involvement of dynein in the pathogenesis of Alzheimer's disease (AD) is thought to be mediated through two proteins, dynactin and Rab5. Dynactin is a protein complex that works closely with dynein to facilitate cargo movements along MTs (Chen et al., 2014). In AD, studies have shown an increased accumulation of AD-associated proteins in axon terminals and a significant increase in dynactin. Rab5 is a small GTPase responsible for the regulation of endocytosis, which depends on dynein for endocytosis and stimulates the endocytic pathway (Kimura & Yanagisawa, 2018). An increase in Rab5 is associated with increased intracellular amyloid β (αβ) plaque formation (Chen et al., 2014), one of the hallmark pathological features of AD (Kimura & Yanagisawa, 2018). Overall, dynein dysfunction has a substantial impact on various neurological and degenerative disorders, emphasizing it is importance in maintaining proper neuronal function and cellular homeostasis.

### 1.2 Structural Components and Motility of Dynein

Dynein is a complex homodimeric protein that comprises two heavy chains (HCs), each weighing approximately 530 kDa, two light intermediate chains (LICs) with a weight of around 74 kDa each, four intermediate chains (ICs) that weigh between 53 kDa and 59 kDa, and six light chains (LCs) that weigh between 10–14 kDa each. The light chains are

involved in cargo binding, whereas the heavy chains contain the motor domain responsible for dynein's motility. The heavy chain of dynein is multifaceted, composed of the tail, linker, hexameric head, buttress, and stalk domains; the latter is attached to the MTBD. Notably, the N-terminus of the dynein, representing approximately one-third of the heavy chain's total mass, comprises the tail and the linker. The motor domain, in particular, houses the AAA+ ATPase motor domain, the stalk, the buttress, and the linker domains (Burgess et al., 2003;Tati & Alisaraie, 2021, Figure 1).

**Figure 1**

*Cytoplasmic Dynein Motor Domain with αβ-Tubulin Dimer, Highlighting Stalk, α-Helices, MTBD, and Colored AAA+ ATPase Modules*

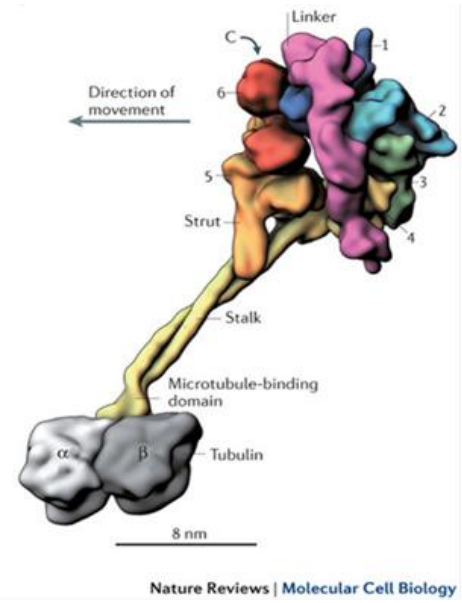


*Note.* Special emphasis is placed on the detailed arrangement of the stalk and the two long α-helices, each rendered separately. Located beneath the stalk is the microtubule-binding domain (MTBD). The figure also provides a numerical identification of the six AAA+ modules, illustrated as a sequence of circles at the top of the structure. Each AAA+ ATPase module is depicted in a distinct colour: AAA+ ATPase 1 (purple) (1), AAA+ ATPase 2 (light blue) (2), AAA+ ATPase 3 (dark green) (3), AAA+ ATPase 4 (yellow) (4), AAA+ ATPase 5 (orange) (5), and AAA+ ATPase 6 (red) (6) and linker element(magenta). From "Functions and Mechanics of Dynein Motor Proteins" (p.715), by A.J. Roberts et al., 2013, Nature Reviews Molecular Cell Biology. Copyright 2013 by Nature Reviews Molecular Cell Biology. Reprinted with permission.

The stalk, which is composed of two interacting α-helices, and the linker, a small protein, work together to transmit conformational changes and coordinate enzymatic functions in dynein motility. The buttress provides additional support and stability, ensuring the proper function of ATP hydrolysis (Burgess et al., 2003; Dutta & Jana, 2019). Crucially, at the terminal of the stalk is the Microtubule-Binding Domain (MTBD), which enables dynein's binding and movement along the microtubule track (Burgess et al., 2004; Carter, 2013). MTBD of dynein 1 is a critical component of the motor protein's structure, playing a pivotal role in its interaction with microtubules. Structurally, the MTBD is composed of six alpha helices (H1- H6), forming a compact, globular structure that is capable of binding to the microtubule surface (Redwine et al., 2012).

Dynein's movement involves four steps: ATP binding, linker shift, ATP to ADP hydrolysis, and phosphate and ADP release. (Figure 2) Initially, ATP binds to the AAA1 module on the motor domain, triggering a conformational change in dynein (Roberts et al., 2009; Manna et al., 2020). This change drives the linker to shift forward, causing the MTBD to "walk" along the microtubule as ATP is hydrolyzed into ADP (Lin et al., 2014; Manna et al., 2020). Finally, the release of a phosphate and ADP resets dynein for another cycle of ATP binding and hydrolysis. The interaction of the MTBD-stalk with the α, βtubulin heterodimer to dynein's movement and function in maintaining intracellular transport and cellular processes is a significant topic of interest. (Figure 1)

**Figure 2.**

*Stages and Conformational Changes in Dynein Motility*

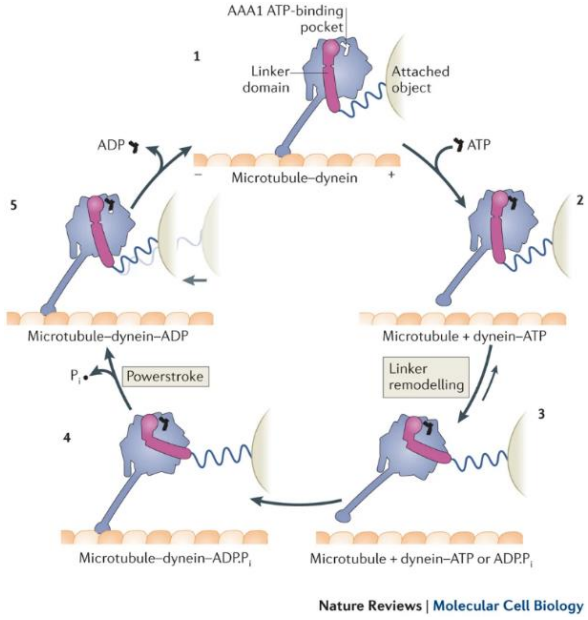


*Note.* The five stages of motility of the dynein motor domain highlighting how it interacts with the microtubule's polarity, which is indicated by plus and minus signs. When there is no nucleotide bound at the AAA1 ATPase site (1), dynein binds tightly to the microtubule. ATP binding triggers it is quick dissociation (2), followed by ATP-driven remodelling of the linker domain, which extends the search range of the MTBD along the microtubule (3). After ATP hydrolysis, the motor domain weakly interacts with a new microtubule binding site (4). With stronger binding, Pi releases from AAA1, straightening the linker and signifying the force-transmitting power stroke (5). ADP-release from AAA1 resets the cycle. From "Functions and Mechanics of Dynein Motor Proteins" (p.718), by A.J. Roberts et al., 2013, Nature Reviews Molecular Cell Biology. Copyright 2013 by Nature Reviews Molecular Cell Biology. Reprinted with permission.

### 1.3 Importance and Dynamics of Microtubules

MTs serve a vital function in neurons; they provide structural support, facilitate intracellular transport, promote axonal growth and direction, aid in neuronal migration, and support cell division. Mammalian MTs are composed of a mixture of isotypes; currently, there are eight α-tubulin isotypes and β-tubulin human isotypes (Vemu et al., 2016). An intricate network of microtubule functions and isotypes necessitates precise regulation, a role fulfilled by Microtubule-Associated Proteins (MAPs). MAPs are a diverse group of proteins that play crucial roles in regulating microtubule dynamics and organization within cells (Ramkumar et al., 2018). MAPs are involved in multiple cellular processes, such as cell expansion, intracellular transport, cell polarity, and neuronal development (Ramkumar et al., 2018; Spiliotis, 2010). MAPs include non-motor proteins such as MAP2 and tau, as well as motor proteins like dynein and kinesin. MAPs such as tau are known to interact with CTTs of α- and β-tubulin subunits (Ferro et al., 2020). Post-translation modifications (PTMs) of tubulin play many roles in neuronal function through the regulation of microtubule stability (Janke & Magiera, 2020). PTMs can occur both on the main body of the tubulin protein and tubulin tails (Figure 3). PTMs appearing on the main body include phosphorylation, polyamidation, and acetylation (Janke & Magiera, 2020). PTMs on tubulin tails include polyglutamylation, detyrosination, and polyglycylation (Janke & Magiera, 2020; Verhey & Gaertig, 2007; Yu et al., 2015) (Figure 3).

**Figure 3.**

*Microtubules and the seven PTMs of CTTs.*

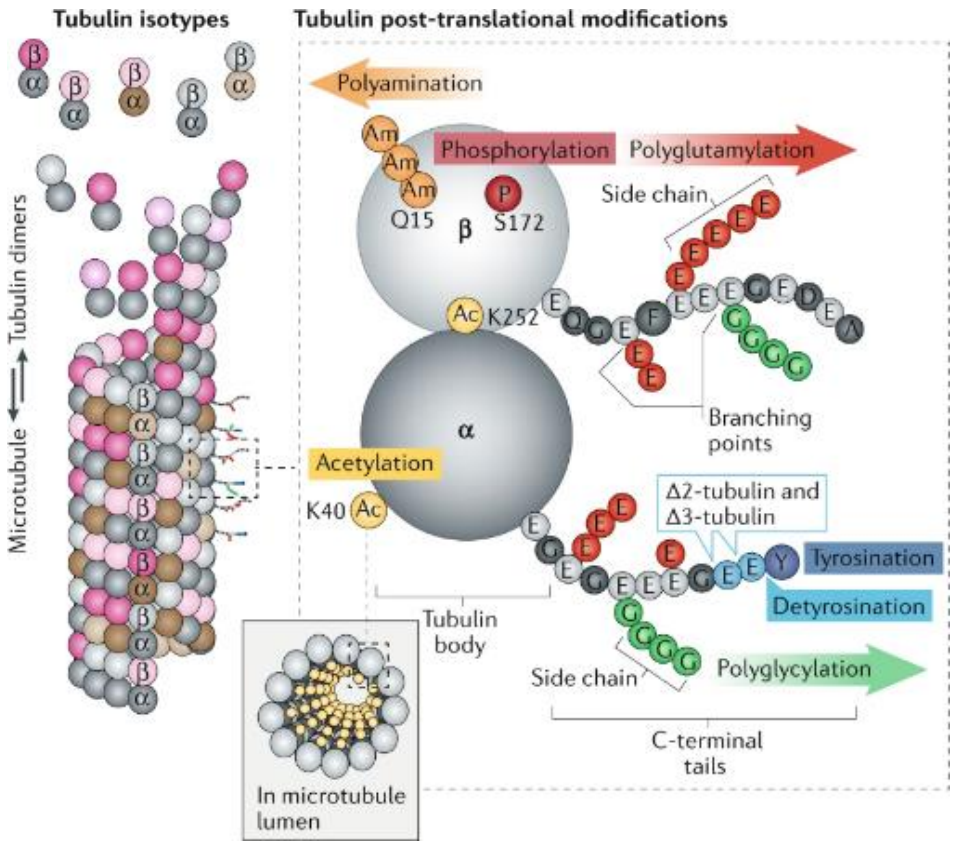


*Note.* Microtubules and post-translational modifications (PTMs) of C-terminal tails (CTTs). Adapted from "The Tubulin Code and It is Role in Controlling Microtubule Properties and Functions" (p.524), by S. Janke & S. Magiera, 2020, Nature Reviews Molecular Cell Biology. Copyright 2020 by Nature Reviews Molecular Cell Biology. Reprinted with permission.

The interactions with CTTs significantly influence the steps involved in the movement of motor proteins such as kinesin (Skiniotis et al., 2004). Similarly, CTTs have been shown to directly interact with or hinder axonemal dynein. Additionally, due to their negative charge, CTTs can electrostatically interact with the MTBD, affecting its affinity for microtubules and potentially influencing its movements (Alper et al., 2014). The flexible nature of CTTs of tubulin plays a role in modulating the motor-tubulin interface of kinesin, which can impact it is processivity and movement (Skiniotis et al., 2004). Given the interactions of CTTs with kinesin and axonemal dynein, it seems plausible to infer that CTTs could also be involved in the binding and motility of cytoplasmic dynein 1The specific interactions, whether direct or via modulation of the motor-tubulin interface, could critically influence the processivity and movement of cytoplasmic dynein-I Therefore, further investigation into this potential relationship would contribute valuable insights into the mechanistic role of CTTs in motor protein function and regulation.

Adding another layer of complexity, polyglutamylation, a PTM of tubulin tails, is linked to reduced motility in retrograde axonal transport. Bodakuntla et al. (2020) investigated the impact of excess MT polyglutamylation on retrograde axonal transport in hippocampal neurons through the deletion of a single de-glut amylase enzyme. Hyperglutamylation led to decreased retrograde transport motility for cargoes such as BDNF, LAMP1, lysosomes, and mitochondria. The authors hypothesized that the PTMs of CTTs might serve to guide and confer specificity for the transport of different cargoes. Although their study did not directly address dynein motility, their findings suggested possible implications for this aspect of transportation.

Ferro et al. (2020) investigated the role of tau protein and negatively charged C-terminal tubulin tails (E-hooks) in dynein binding and motility. First, their findings confirmed tau's competing role for E-hooks; in the absence of E-hooks, the run frequency of dynein was reduced to 50-70%. Furthermore, the combination of 100 nM Tau and the lack of E-hooks completely prevented dynein binding. Tyrosination of C-terminal tails is characterized by reductions in the velocity of dynein motility. Ayloo et al. (2017) investigated the tyrosination of the CTTs, and its effects on the regulation and binding of dynein in organelle-specific dendrites and axons for the trafficking of the BDNF/TrkB-positive signalling endosomes using a novel optogenetic tool. Nocodazole is a drug commonly used to disrupt MT networks in cells; Low doses can alter the balance between tyrosinated and detyrosinated CTTs on MTs (Ayloo et al., 2017). Ayloo et al. (2017) employed nocodazole to investigate the relationship between this balance and dynein function. They compared nocodazole-treated neurons to control neurons and observed a significant reduction in dynein-mediated motility of peroxisomes along the axons of nocodazole-treated neurons. This reduction was accompanied by frequent pauses and a notable decrease in average velocity. The authors also aimed to determine whether this effect was consistent in the dendrites of neurons, and their data indicated similar results, in which, again, a decrease in the average velocity of dynein was observed. In conclusion, *in vitro* studies of dynein are of paramount importance as they allow for a controlled exploration of the protein's structure, function, and interactions (Ayloo et al., 2017).

Salt bridges are characterized as the electrostatic interactions that occur between two opposing charged molecular groups. Salt bridges are found between interacting

proteins, contributing to structural and conformational changes (Ban et al., 2019). Previous research by Heale and Alisaraie (2020) utilized molecular dynamics (MD) simulations to demonstrate the importance of tubulin terminal tails in dynein movement. The simulations were performed between the dynein's MTBD and the α, and β-tubulin heterodimer, including CTTs. Their work highlighted the structural mechanism of salt bridge interactions between β-CTT and β-H18 with the MTBD-H1 and H7 and the crucial role they play in the binding process. Interactions between specific residues such as α-Arg402 (α-H14-H15 loop) with Glu3390 (MTBD-H1) and α-Gly416 (H16) with Arg3469 (MTBD-H7) were also highlighted to be crucial in enabling a structural change called the "registry switch." A registry switch is essential for activating the ATPase activity in dynein. Heale and Alisaraie (2020) indicated that their findings supported the hypothesis proposed by Uchimura et al. (2015) that the formation of salt bridges between MTBD Arg3469 and α-Glu415 might promote high-affinity conformations. High-affinity conformations facilitate stronger interactions between dynein and the MTs, which is essential for efficient movement along the microtubule tracks.

### 1.4 Studying Biological Systems Through Molecular Dynamics Simulations

Molecular Dynamics (MD) simulations are *in silico* methods that employ Newton's equation of motion to numerically determine the dynamic movements of atoms in molecules for a system of interacting particles (McCammon & Harvey, 1987). The interactions between atoms are mathematically modelled using force fields to describe the potential energies of the system as a function of atomic position and allow for the calculation of forces acting on individual atoms (Abraham et al., 2023). The force fields

account for intra and inter-molecular forces (i.e., bonded and non-bonded interactions) (Abraham et al., 2023). An appropriate force field for the system under study is essential to ensure accurate results. Some common force fields include AMBER (Weiner et al., 1986), CHARMM (Vanommeslaeghe et al., 2010), GROMOS (Schuler et al., 2001), and OPLS-AA (Dodda et al., 2017), each having their respective applications (Guvench & MacKerell, 2008). Periodic boundary conditions (PBC) are employed in MD simulations to mimic an infinite system using repeating cell units and to reduce the effects of finite system size. The PBC alleviates issues such as edge effects and assists in achieving an accurate representation of bulk properties (Metropolis et al., 2004).

MD simulations involve five steps: 1. Energy minimization, 2. Position restraint 3. Equilibration 4. MD Data Collection 5. Data Analysis. The equilibration step has multiple standard techniques, such as energy minimization, pressure, and temperature equilibration. Energy minimization is done to relieve any atomic clashes that may arise in the system setup process (Abraham et al., 2023; Leach & AR, 2001). Position restraint is done to prevent the large movements of protein atoms. Position restraint uses harmonic potentials to prevent large movements. The primary purpose of position restraint is to allow the solvent molecules to equilibrate around protein, avoiding atomic clashes (Abraham et al., 2023). The system pressure is equilibrated using the Berendsen barostat to keep the system at constant pressure (Abraham et al., 2023; Leach & AR, 2001). After pressure equilibration, the temperature is held constant, allowing for the position and velocities of the atoms to equilibrate; typically, this is done by simulating with small time-steps (e.g., femtosecond scale) until achieving the lowest possible energy according to the

experiment's condition and the values of the parameters (Abraham et al., 2023; Leach & AR, 2001). Once the system has been fully equilibrated, it is finally ready for the MD data collection. MD simulations employ specified integration algorithms, such as Verlet or Leapfrog, to propagate the atoms' positions and velocities (Abraham et al., 2023; Leach & AR, 2001).

MD simulations provide insights into the atomic-level behaviour and interactions of proteins, which are difficult to achieve in many experimental *in vitro* techniques. The details helps a better understanding of the mechanisms governing protein behaviour. MD simulations also enable the observation of protein dynamics and conformational changes over time, providing insights into the molecular mechanisms driving protein function. Most *in vitro,* studies provide static snapshots of protein conformations, which may only partially capture the dynamic nature of proteins. As a result, dynein and it is complex architecture and large structural architecture make computational modelling of the system challenging.

Dynein movement is characterized by variability both in terms of the distances it travels (i.e., length scales) and the speed and duration of it is activities (i.e., time scales), requiring a combination of various computational methods, similar to experimental approaches to thoroughly investigate the mechanochemical cycle (Dutta & Jana, 2021).

## 2. Methods

The α, β tubulin heterodimer structure was obtained from the Protein Data Bank (PDB) under the code 5JCO (Vemu et al., 2016). This structure represented single-isoform recombinant neuronal human tubulin, from which an α, β-heterodimer was isolated. Incomplete C-terminal tails were then built onto this structure by a lab member. The

structure of the MTBD and the stalk domain was also obtained from the PDB with code 3VKG (Kon et al., 2012). The MTBD and thestalk domain's structural model for the studied species was built using homology modelling by the PI. MD simulations were conducted to investigate and analyze the protein subunits' conformational changes and movements utilizing Groningen MAchine for Chemical Simulations (GROMACS) v. 2022.1 software package (Abraham et al., 2023). GROMACS employs the Newtonian equation of motion to numerically determine the dynamic motions of all the atoms in a system of interacting molecules (Abraham et al., 2023). GROMOS 54A7 Force field was used to assemble the topology data for the atoms in the system (Schmid et al., 2011). The system was solvated in a water box using the SPC water model, and 50 sodium ions were added ($Na^+$) to neutralize the proteins' net charge. Following solvation, proteins were centred in a cubic box at a distance of 1.0 nm from the edge, with a total volume of 1981.3 $nm^3$. Energy Minimization (EMin) was conducted using the steepest descent (SD) algorithm (Leach & AR, 2001) to remove atomic clashes. Particle Mesh Ewald (PME) was employed for longer-range interaction calculations (Essmann et al., 1995). The position restraint (PR) or NVT phase of the MD simulations ran for 1000 ps (i.e., 1 ns) with a 0.002 ps step size, using the "md" integrator and the LINear Constraint Solver (LINCS) algorithm (Hess et al., 1997) to restrain all bonds. The velocity rescaling thermostat (Bussi et al., 2007) relaxed the system temperature to 300.0 K. Equilibration (EQ) phase, the "md" integrator was employed with a step size of 0.002 ps and 800.0 ns to integrate Newton's equation of motion was the initial goal.

Compressibility was set to $4.5\times10^{-5}$ bar, and a constant pressure of 1.0 bar was attained through the Berendsen pressure coupling. MD simulations employed the "md" integrator once more, with calculations being conducted for ~ 319.5 ns at increments of 0.002 ps. The MD simulations were carried out using Graham, a High-Performance Computer Cluster provided by the Digital Research Alliance of Canada. All simulation data were analyzed using the MDAnalysis package (version 2.2.0) in Python (Gowers et al., 2016; Michaud-Agrawal et al., 2011). For the visualization of molecular structures and to create images for this study, PyMOL was employed (Schrödinger, LLC, 2015).Visual Molecular Dynamics (VMD) algorithm was utilized for salt bridge analysis (Humphrey et al., 1996).

*This research is a qualitative analysis based on a 320 ns length trajectory. Given the inherent time constraints, the simulations performed for this study did not progress convergence and the later stages of the simulation.*

## 3. Results

The structural framework utilized for this study was adapted from Protein Data Bank entry 5JCO, a model solved to a resolution of 4.2 Å. The α-tubulin component of the dimer is composed of 18 helices (H1–H18) and 11 beta strands (B1–B11), with a combined total of 451 residues. β-tubulin is comprised of 9 β-strands (B1-B9) and 18 α-helices (H1-H18) with a combined total of 450 residues.

MTBD of the dynein motor protein is prominently positioned on the dorsal side of the tubulin dimer, interfacing both α- and β-tubulin subunit; the representation differentiates

the system's various elements and emphasizes the strategic positioning of the MTBD in dynein-tubulin interactions. (Figure 4). The MTBD consisted of seven helices (H1-H7): H1 (Gln3302-Ser3309), H2 (Ala3315-Leu3328), H3 (Trp3335-Ile3342), H4 (Pro3349-Asn3353), H5 (Ala3356-Glu3358), H6 (Asp3361-Ser3373), and H7 (Tyr3379-Ala3385). The main helices situated at the interface between the Microtubule and the Microtubule Binding Domain (MT-MTBD), identified as MTBD-H1(Gly 3302-Ser 3309), MTBD-H3(Trp 3335 - Ile 3342), and MTBD-H7 (Tyr 3379 – Ala 3385). (Figure 5). A visual comparative analysis was performed on the protein's conformation at 0 ns time frame and the conformation from the last frame at 319.5 ns; their superimpositin allowed to discern the significant changes that occurred during the simulation period. This visualization aids in identifying key structural shifts in (MTBD-H1, H2, H3, H4 and H7) and in interpreting their potential impact on system performance. (Figure 6-7)

**Figure 4.**

*Initial Configuration of the Dynein-Tubulin System Highlighting Key Components and Interaction Complexity*

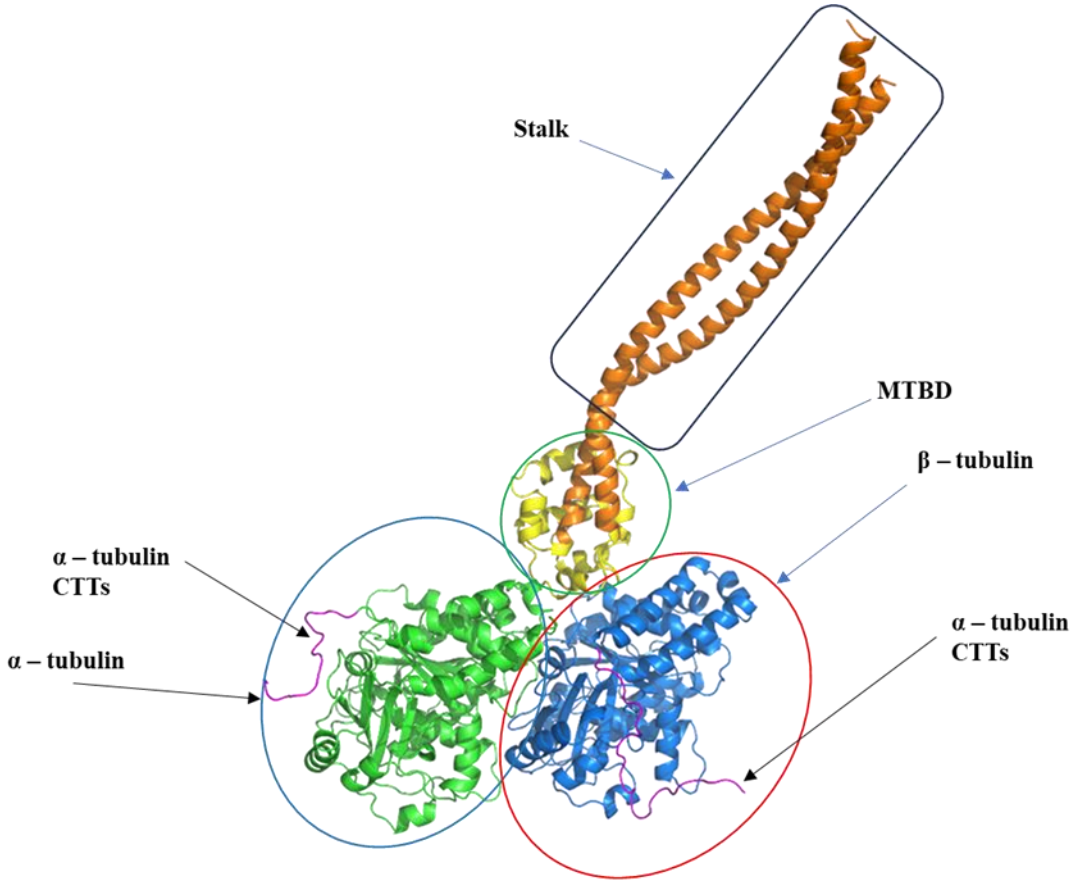


*Note.* Conformation of the initial system from energy minimization and pressure stabilization. The microtubule-binding domain (MTBD) is positioned towards the dorsal side, and the two long α-helices of the stalk are arranged in detail. The dynein stalk (orange), the MTBD (yellow), α-tubulin (green), β-tubulin (blue), and the C-terminal tails (CTTs) of both α- and β-tubulin in magenta, making it easy to distinguish between the different system components.

**Figure 5**

*Color-Coded Representation of Dynein's MTBD Helices*

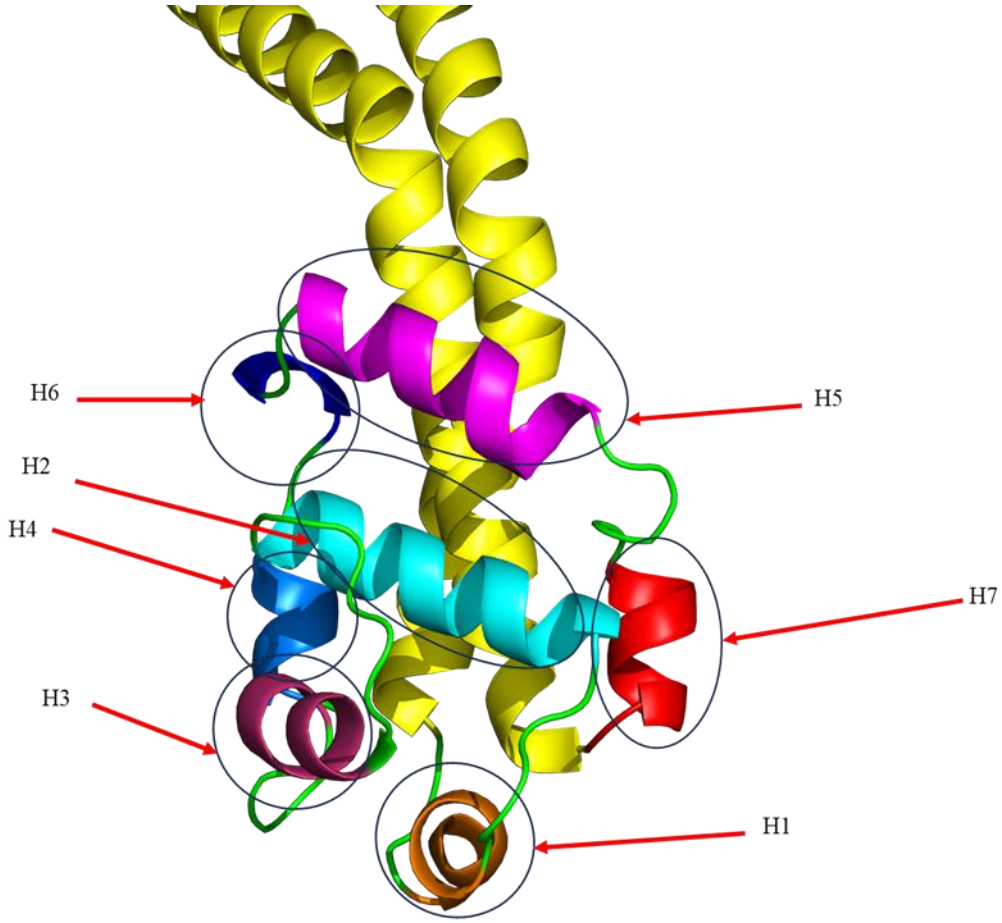


*Note.* The structure of dynein's microtubule-binding domain (MTBD), with its various helices distinctively colored for clarity. The helices are displayed as follows: MTBD-H1 (orange), MTBD-H2 (cyan), MTBD-H3 (dark pink), MTBD-H4 (light blue), MTBD-H5 (magenta), MTBD-H6 (dark blue), and MTBD-H7 (red). The use of color coding allows for easy differentiation and identification of each helix within the MTBD structure.

**Figure 6.**

*Superimposed Structures of the Initial and Final System States Following Simulation*

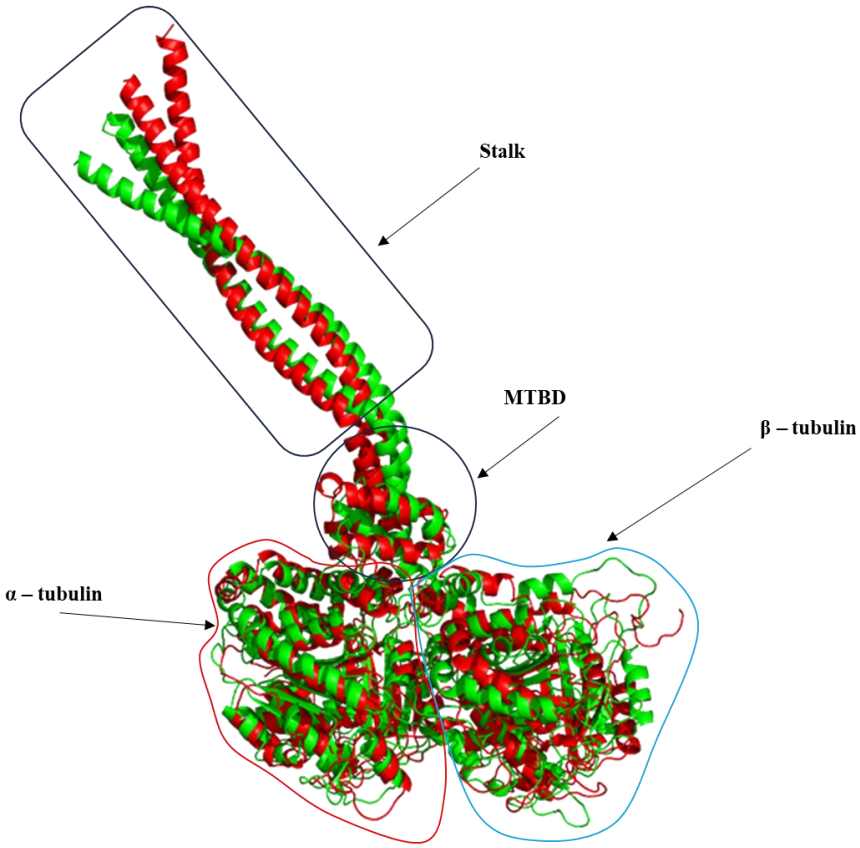


*Note.* The superimposition of the conformations from 0 ns time frame and 319.5 ns confromation. The conformation at 0 ns (red), at 319.5 ns (green).

*This is only a qualitative comparison; otherwise, frames before convergence are not analytically worthwhile.*

**Figure 7**

*Comparative Analysis of MTBD Helical Shifts: Superimposed Conformation at 0 ns and 319.5 ns Simulation Timepoints*

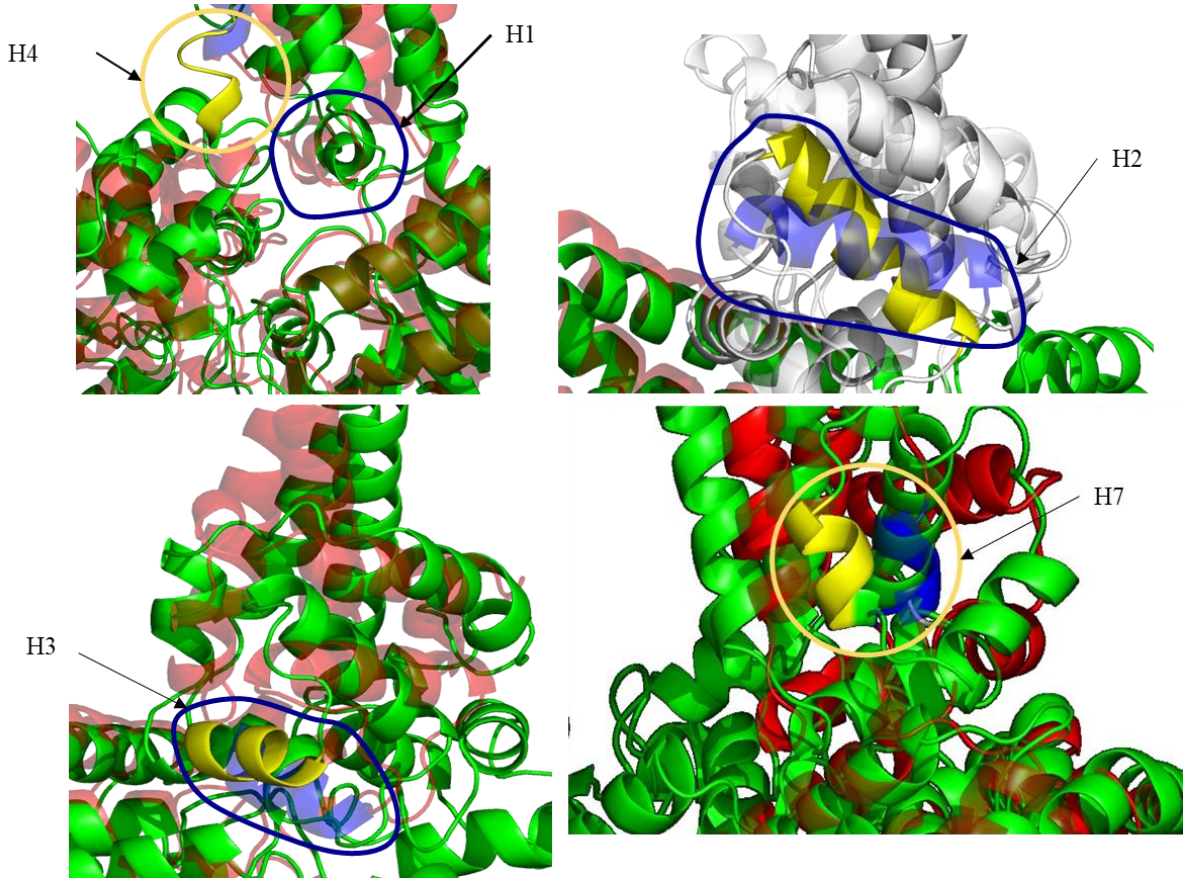


*Note*. The shifts observed in the helices H1, H2, H3, H4, and H7 of the Microtubule Binding Domain (MTBD) from the start to the end of the simulation (0 ns to 319.5 ns). The changes in position and orientation of these helices reflect the structural dynamics of the MTBD in the studied time period.

### 3.1 RMSD Analysis of System Components

The structural stability, conformational changes of different components and the convergence of the dynein-tubulin system were analyzed by calculating the Root Mean Square Deviation (RMSD, Knapp et al., 2011). The average RMSD of the 319.5 ns length MD trajectory for the entire system (i.e., tubulins, the MTBD and stalk) , including all components, is ~7.53 Å. After the removal of the dynein's highly flexible stalk domain and the C-terminal tails of the tubulins from the system, the average RMSD decreases to about 3.70 Å.The average RMSD for α-tubulin (excluding the C-terminal tail) was ~3.49 Å. The average RMSD of β-tubulin was around 2.74 Å. The RMSD analysis of α-CTTs indicated an average RMSD of 5.39 Å and an RMSD analysis of β-CTTs indicated an average RMSD of 7.29 Å for the CTT of beta-tubulin (Figure 8-13).

**Figure 8.**

*RMSD of the Complete system including CTTs and Dyenin Stalk*

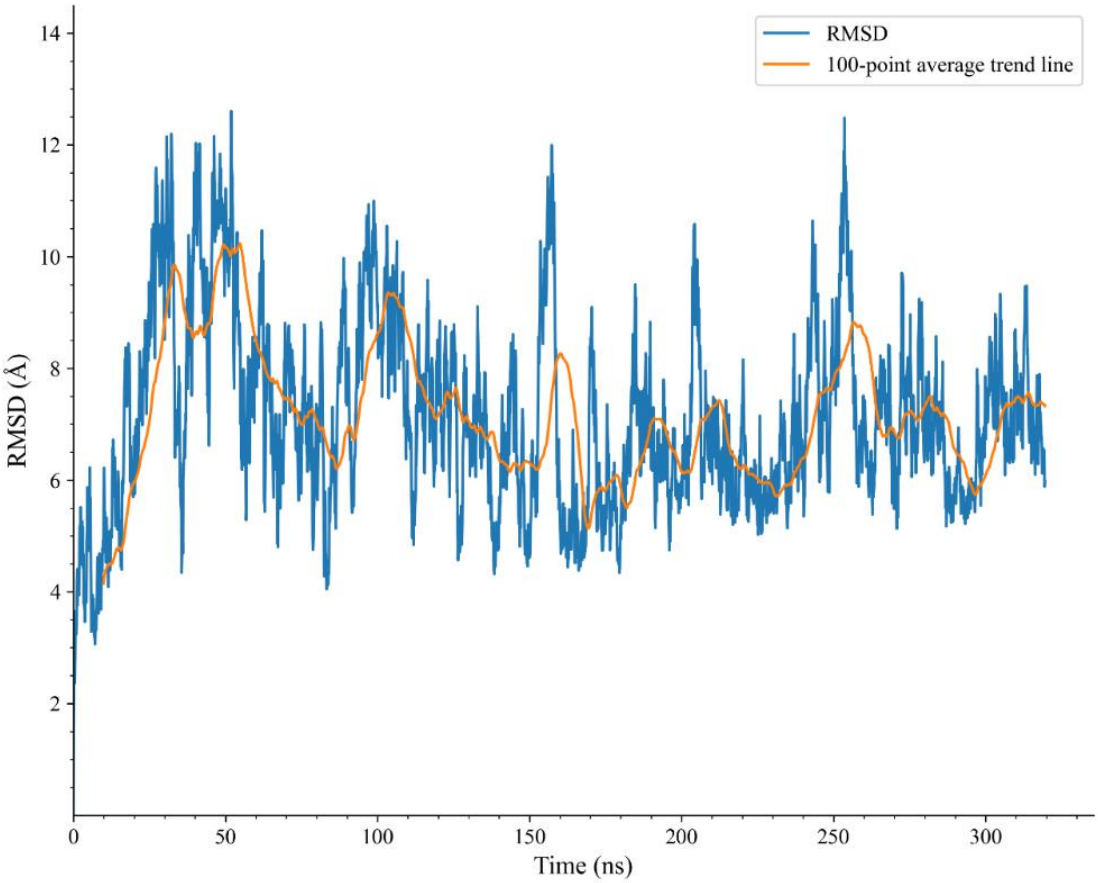


*Note.* The dark blue line represents the raw RMSD data (blue), 100-point average (orange). The time range of the trajectory assessed for the RMSD calculations spanned from 0 ns to 319.5 ns. The y-axis indicates the RMSD value in Angstroms (Å).

*This is only a qualitative comparions otherwise frames prior to convergnace are not analytically worthwhile.*

**Figure 9.**

*Stability Analysis of Dynein-Tubulin System and Impact of CTTs and Stalk on RMSD Fluctuations*

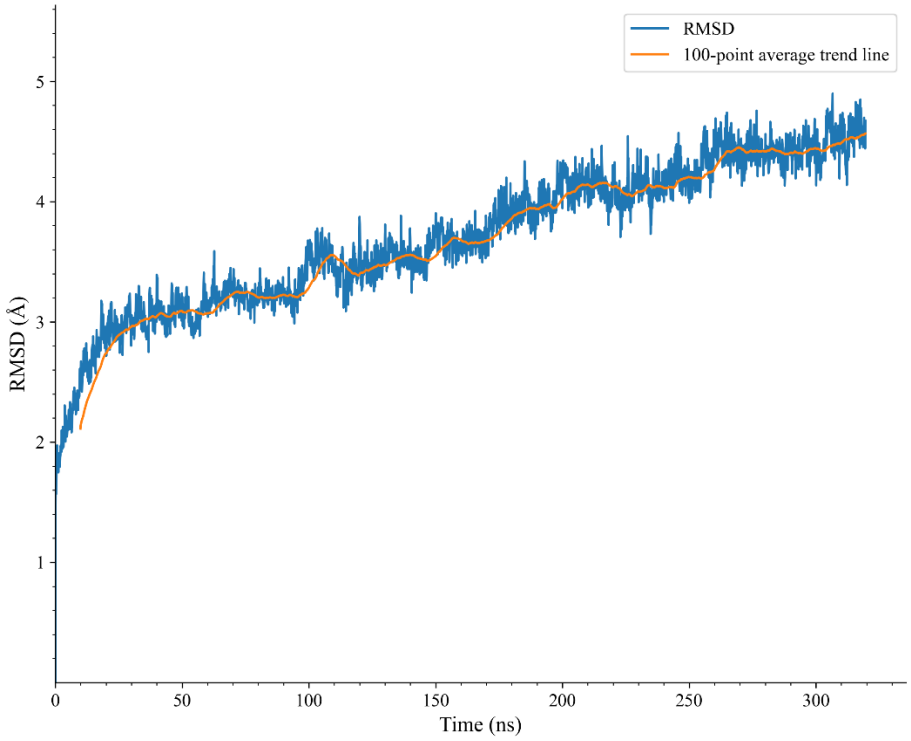


*Note.* The dark blue line represents the raw RMSD data for all proteins'components excluding CTTs and stalk. The orange line is a trend line depicting the 100-data point average. The time range for the RMSD measurements spanned from 0 ns to 319.5 ns of the MD trajectory. The y-axis indicates the RMSD value in Angstroms (Å).

*This is only a qualitative comparions otherwise frames prior to convergnace are not analytically worthwhile.*

**Figure 10.**

*RMSD of α-tubulin*

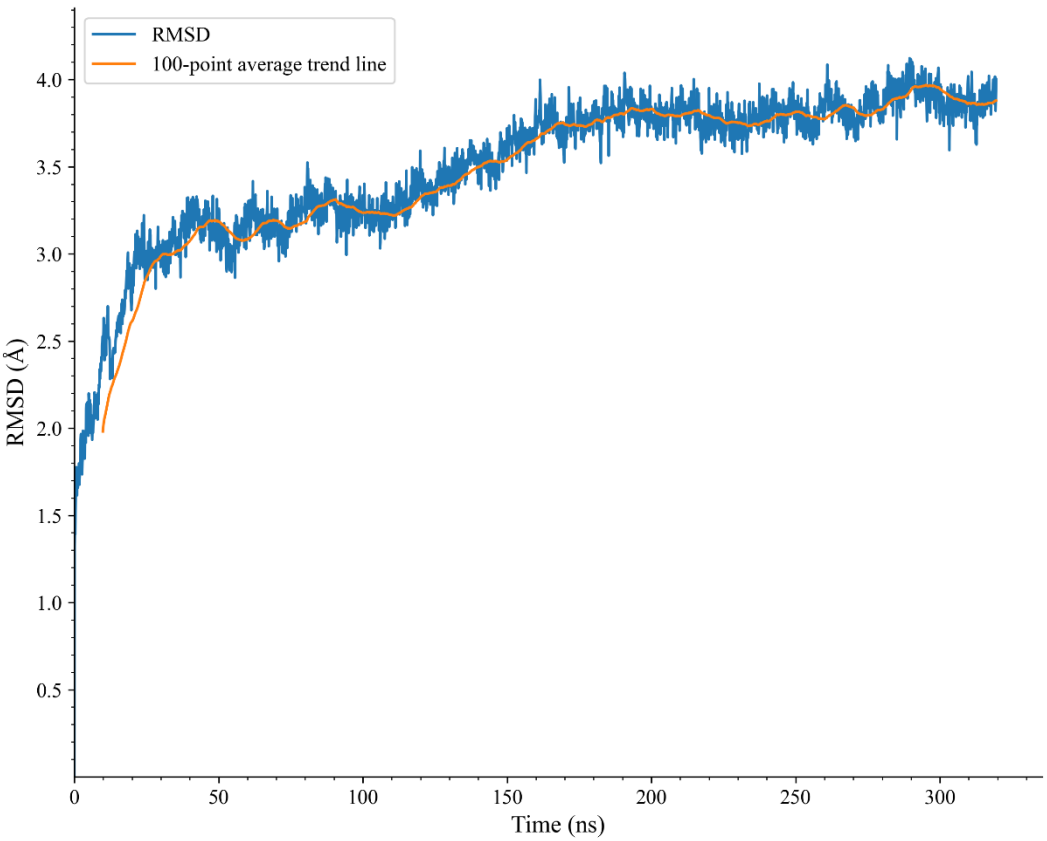


*Note.* The dark blue line represents the raw RMSD data for α-tubulin. The orange line is a trend line depicting the 100-point average. The time range for the RMSD measurements spanned from 0 ns to 319.5 ns. The y-axis indicates the RMSD value in Angstroms (Å). *This is only a qualitative comparions otherwise frames prior to convergnace are not analytically worthwhile.*

**Figure 11.**

*RMSD of β-tubulin*

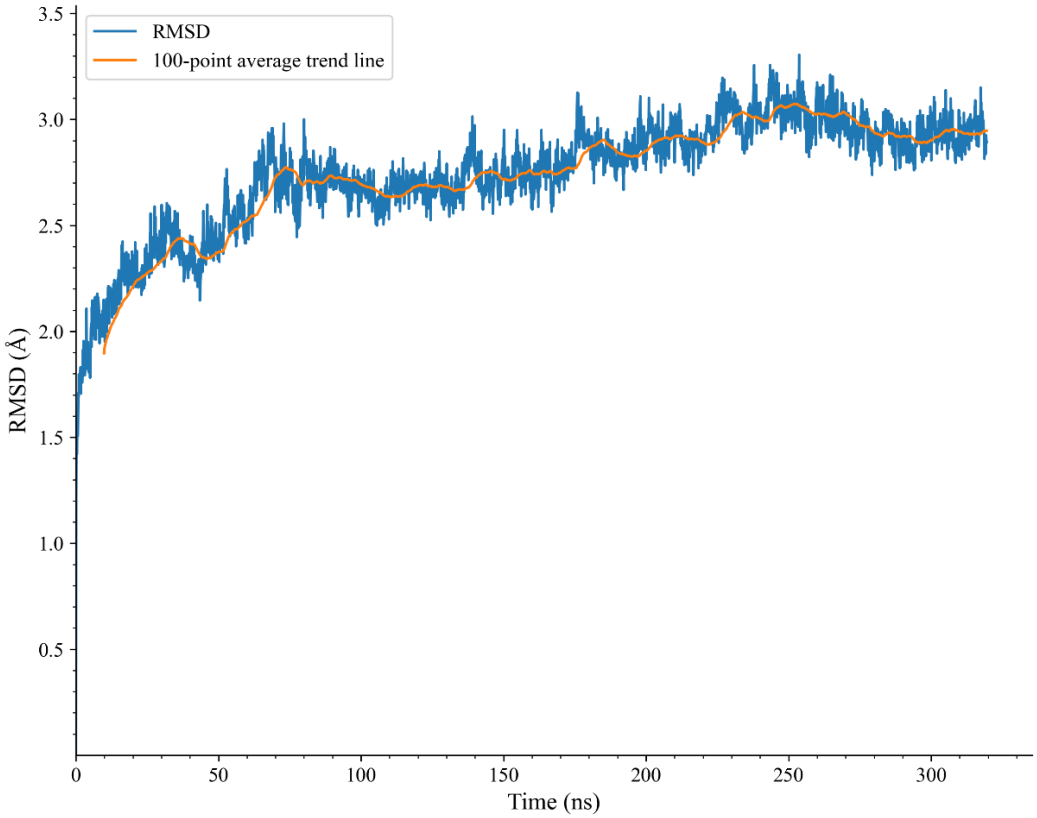


*Note.* The dark blue line represents the raw RMSD data for β-tubulin. The orange line is a trend line depicting the 100-point average. The time range for the RMSD measurements spanned from 0 ns to 319.5 ns. The y-axis indicates the RMSD value in Angstroms (Å).

*This is only a qualitative comparions otherwise frames prior to convergnace are not analytically worthwhile.*

**Figure 12.**

*RMSD of α-CTT*

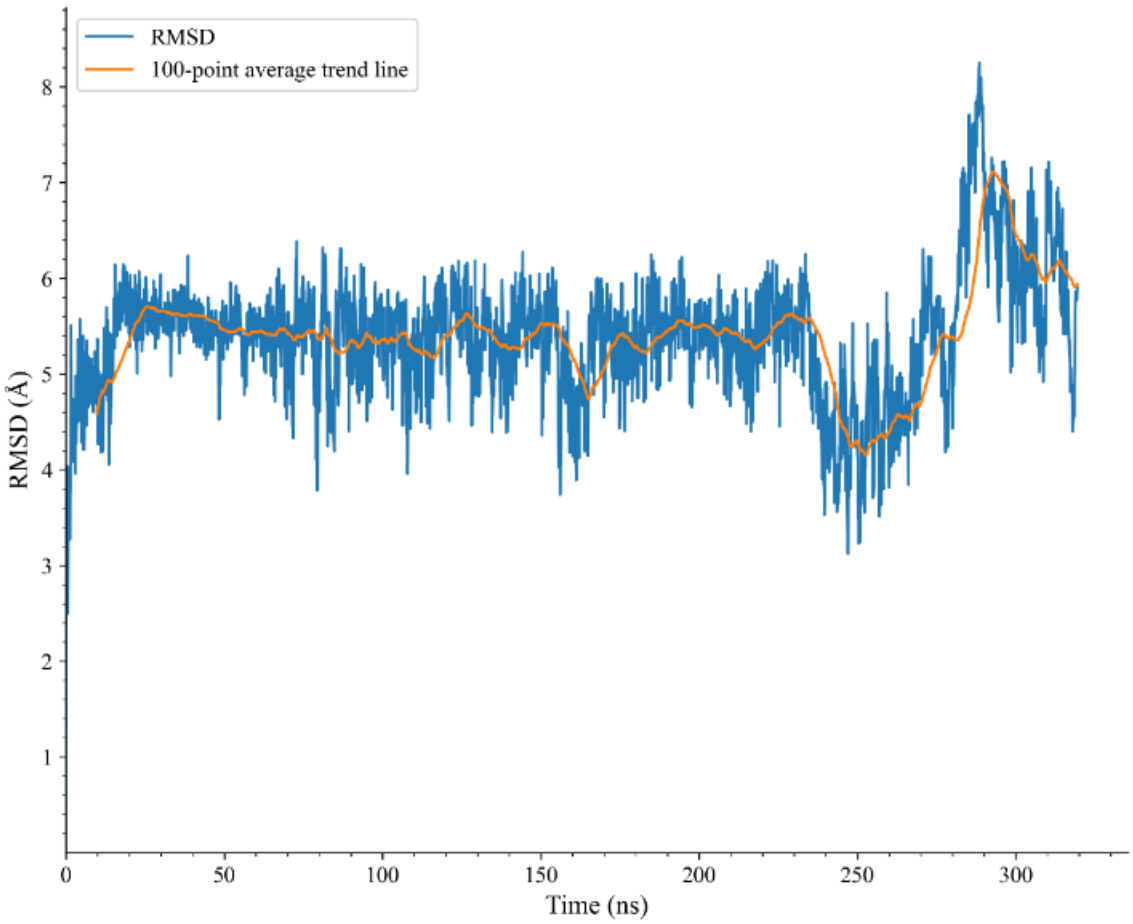


*Note.* The dark blue line represents the raw RMSD data for α-CTT. The orange line is a trend line depicting the 100-point average. The time range for the RMSD measurements spanned from 0 ns to 319.5 ns. The y-axis indicates the RMSD value in Angstroms (Å).

*This is only a qualitative comparions otherwise frames prior to convergnace are not analytically worthwhile*

**Figure 13.**

*RMSD of β-CTTs*

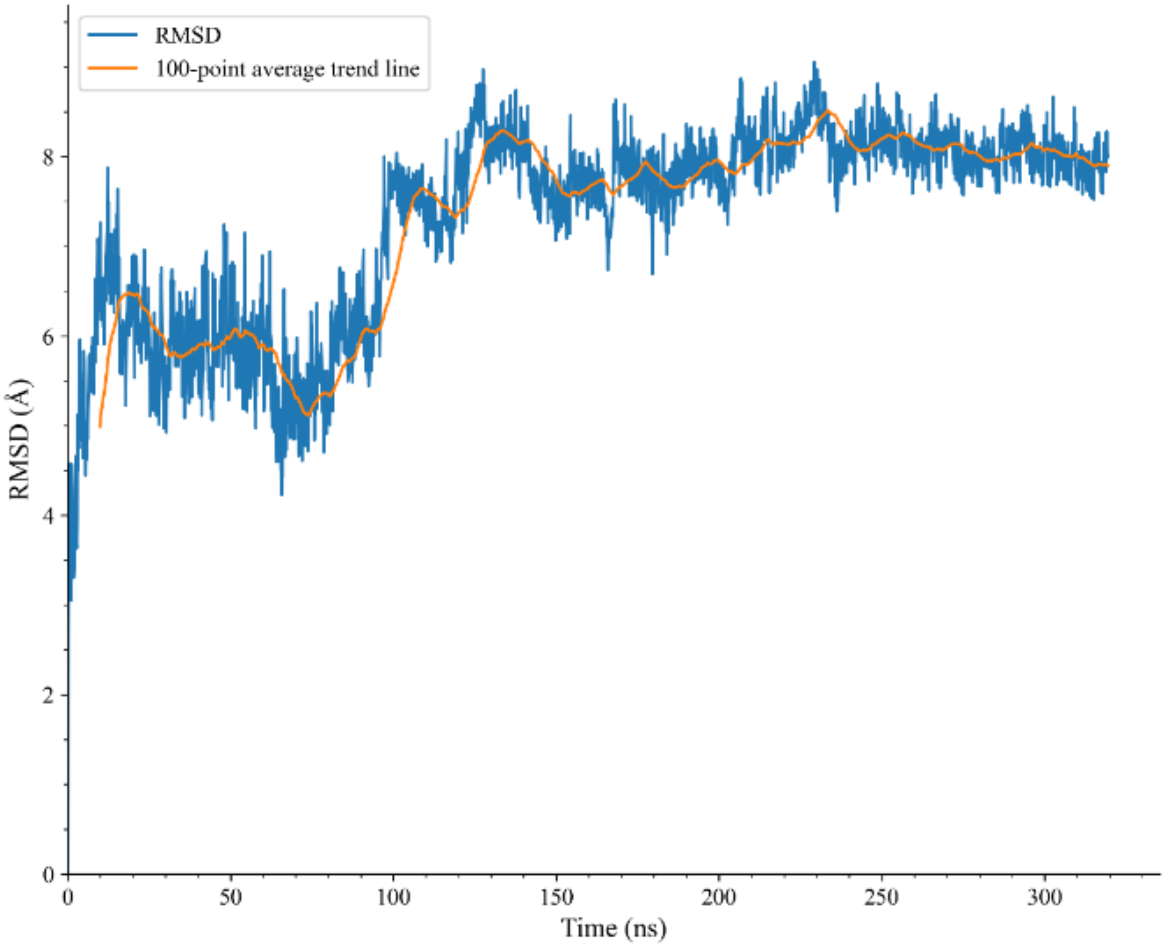


*Note.* The dark blue line represents the raw RMSD data for β-CTT. The orange line is a trend line depicting the 100-data point average. The time range for the RMSD measurements spanned from 0 ns to 319.5 ns. The y-axis indicates the RMSD value in Angstroms (Å).

*This is only a qualitative comparions otherwise frames prior to convergnace are not analytically worthwhile.*

### 3.2 RMSF Analysis of System Components

The Root Mean Square Fluctuation (RMSF) of α- and β-tubulin residues and helices in the MTBD of dynein were investigated to determine the flexibility of these components during the MD simulation of MTBD-tubulin heterodimer (Figure 14-15). The amino acid residue LYS 338, found in the α-tubulin protein, showed the highest RMSF value of 9.28 Å, indicating that it experienced the greatest amount of fluctuation and therefore had the most flexibility during the simulation. The residues with the next highest RMSF values were THR 337 and ARG 339, with 9.06 Å and 9.04 Å, respectively (Figure 14).

The RMSF value for residue GLU 401 in β-tubulin was the highest at 7.38 Å. Following this were residues TYR 106 (7.30 Å), ALA 97 (7.27 Å), ASN 99 (7.20 Å), and HIS 396 (7.18 Å). Other residues with high RMSF values included GLY 96 (7.17 Å), LYS 392 (7.16 Å), LYS 103 (7.16 Å), GLY 400 (7.15 Å), and GLY 402 (7.04 Å), certain residues that are more prone to fluctuations in β-tubulin (Figure 14).

RMSF values for the helices in the MTBD H1 had an average RMSF value of 4.9 Å, with VAL 3307 being the most flexible residue (RMSF of 5.10 Å) and VAL 3305 being the least (RMSF of 4.59 Å). MTBD H2 and H3 also had high RMSF values in specific residues (ALA 3315 in H2 and LYS 3336 in H3). The analysis of MTBD H4, H5, and H7 revealed similar findings. For instance, the highest RMSF value in the MTBD H4 was 5.21 Å at Phe3347, while the lowest was 4.76 Å at Pro3349. Similarly, helix H5 had the highest RMSF value of 6.76 Å at Lys3369 and the lowest value of 5.78 Å at Ile3363. Lastly, Glu3380 had the most dynamic behaviour with an RMSF of 5.97 Å within helix H7, while Ala3385 was the most rigid residue in this region with an RMSF of 5.01 Å (Figure 15).

**Figure 14.**

*RMSF of Heterodimer throughout 319.5 ns*

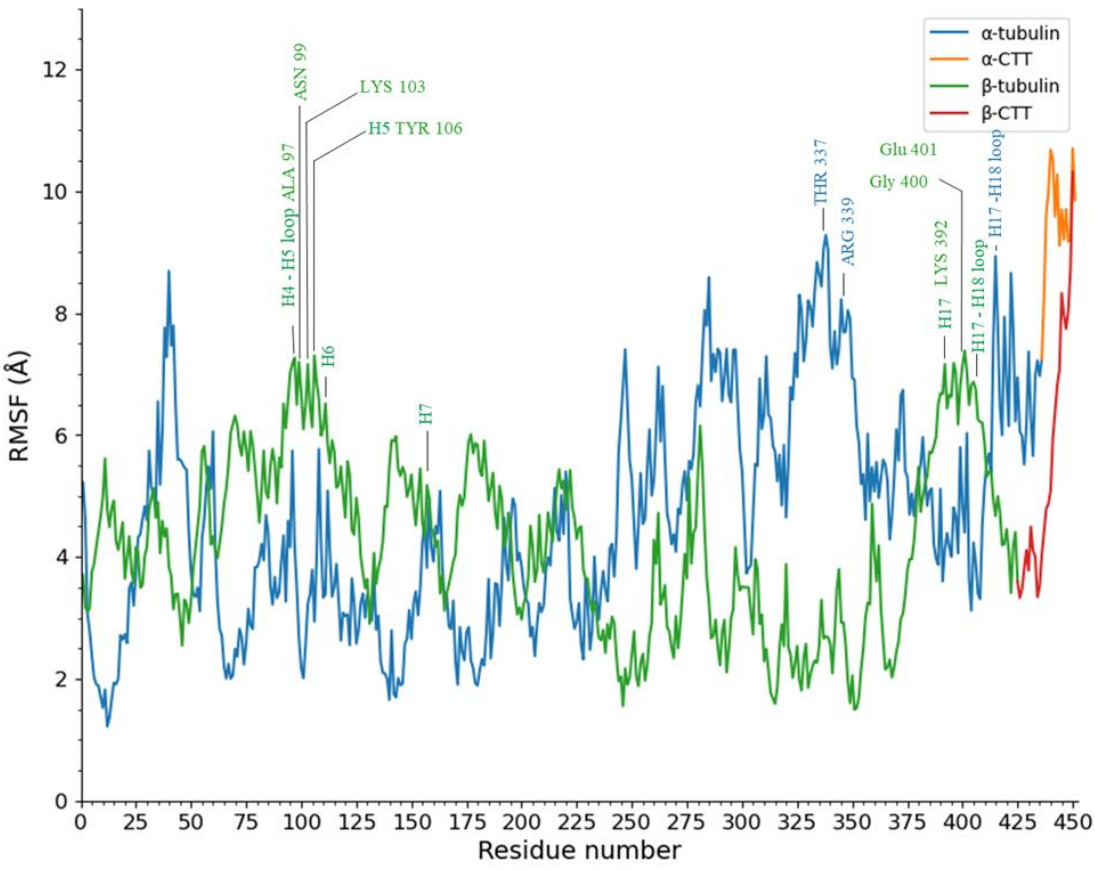


*Note.* The figure depicts the RMSF of tubulin residues throughout the course of the simulation. Each point on the graph corresponds to a specific residue in the α-tubulin shown in blue or β-tubulin shown in green, and their CTT is shown in orange and red, respectively. The y-axis indicates the RMSF value in Angstroms (Å).

*This is only a qualitative comparions otherwise frames prior to convergnace are not analytically worthwhile.*

**Figure 15**

*Root-Mean-Square Fluctuation (RMSF) of Microtubule-Binding Domain (MTBD) Residues*

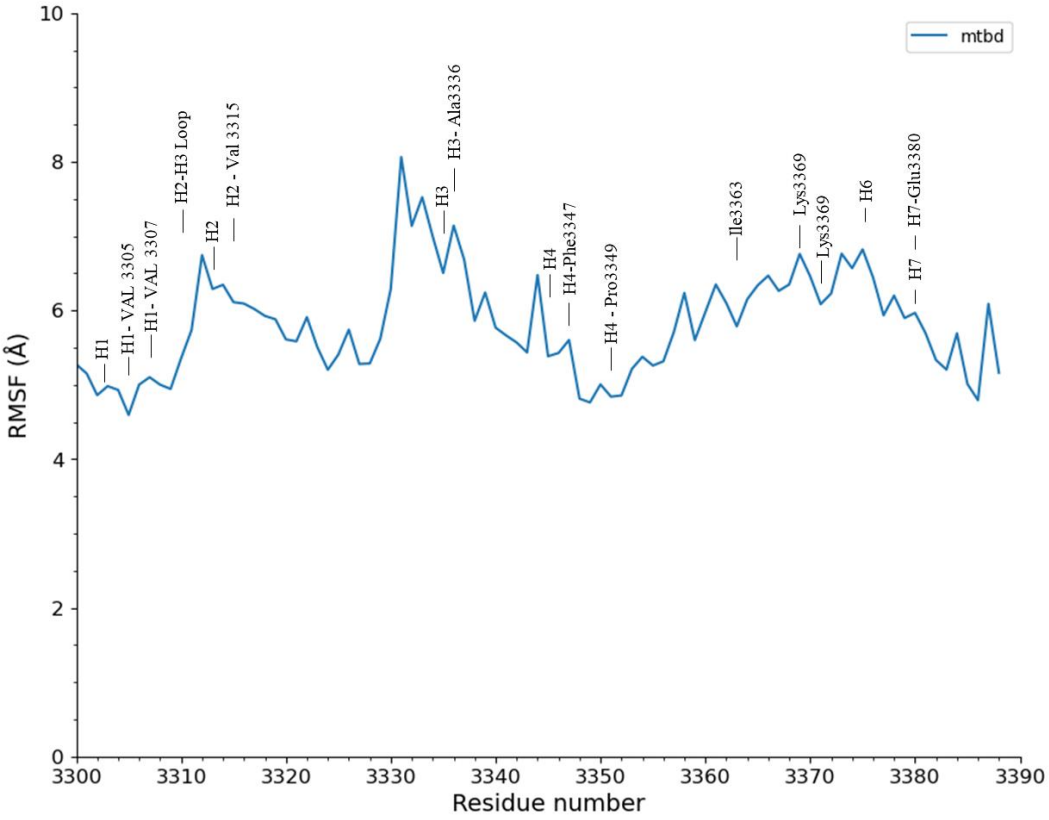


*Note.* The figure depicts the RMSF of MTBD residues throughout the course of the simulation. Each point on the graph corresponds to a specific residue in the MTBD, with the y-axis indicating the RMSF value in Angstroms (Å).

*This is only a qualitative comparions otherwise frames prior to convergnace are not analytically worthwhile.*

### 3.3 dCOM Analysis of Potential Interactions between System Components

The distance between Center of Mass (dCOM) of different domains and segments of the proteins in the system (i.e., MTBD structure, the α- and β-tubulin components and their respective CTTs) were calculated to determine the potential interactions between the system components.

Over time, there were changes in the distances between different parts of the tubulin molecule. Specifically, the dCOM between the MTBD and α-tubulin decreased from 46.5 Å to 44.9 Å. While the dCOM between the MTBD and CTT of α-tubulin decreased from 66.9 Å to 60.5 Å. On the other hand, the dCOM between the MTBD and β-tubulin decreased from 34.5 Å to 34.0 Å while the distance between the MTBD and CTT of β-tubulin only slightly decreased from 52.8 Å to 52.0 Å. Those changes were observed over a period of approximately 319.5 ns. (Figure 16 and 17 ).

The position of the H1-H7 of the MTBD versus the CTTs of α- and β-tubulin were inspected. The dCOM was calculated to assess the possibility of the interaction between these components. The dCOM between the CTT of α-tubulin and MTBD-H7 decreased from 56.4 Å to 46.3 Å, while the dCOM between the CTT of β-tubulin and the MTBD-H3 increased from 49.9 Å to 52.0 Å (Figure 18 and 19).

After analyzing the dCOM between the MTBD helices (H1-H7) and α- and β-tubulin, it was found that most interactions resulted in a decrease in the dCOM. The largest decrease was observed for the interaction between MTBD-H5 and α-tubulin (from 77.6 Å to 63.7 Å)(Figure ). However, the interaction between MTBD-H3 and β-tubulin resulted in

an increase in the dCOM (from 49.1 Å to 52.0 Å). Although interestingly the there a decreased dCOM between MTBD-H1 and β-tubulin from 23.9 Å to 22.8 Å (Figure 20-23).

**Figure 16.**

*dCOM Analysis of Between Tubulins and MTBD*

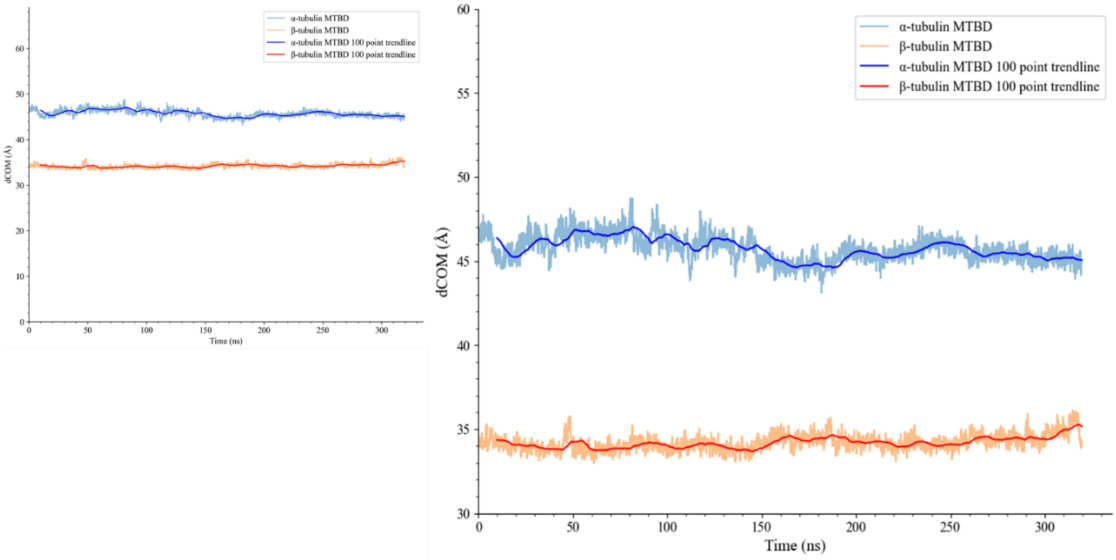


*Note.* The light blue line represents the original dCOM values for α-tubulin, while the orange line illustrates the dCOM of α-tubulin and the Microtubule Binding Domain (MTBD). The dark blue line serves as the 100-point average trend line for α-tubulin, and the red line is the 100-datapoint average trend line for β-tubulin.

*This is only a qualitative comparions otherwise frames prior to convergnace are not analytically worthwhile.*

**Figure 17.**

*dCOM Analysis Between Tubulin CTTs and MTBD*

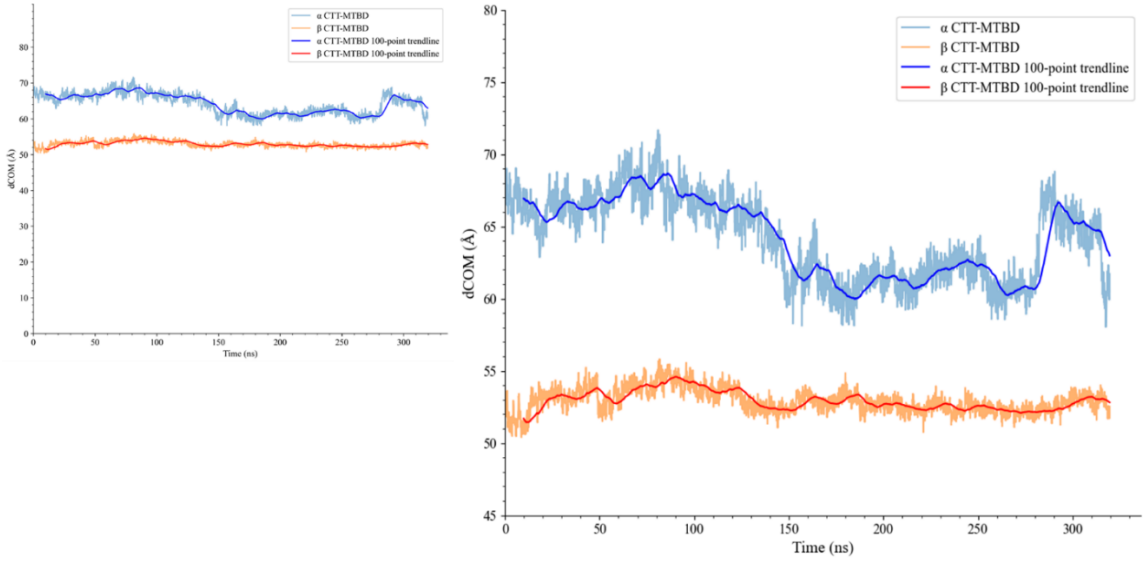


*Note.* The light blue line represents the original dCOM values for α-tubulin CTT, while the orange line illustrates the dCOM of β-tubulin CTT and the Microtubule Binding Domain (MTBD). The dark blue line serves as the 100-datapoint average trend line for α-tubulin CTT, and the red line is the 100-datapoint average trend line for β-tubulin CTT.

*This is only a qualitative comparions otherwise frames prior to convergnace are not analytically worthwhile.*

***Figure 18***

*dCOM Analysis of Between Tubulin CTTs and MTBD-H7*

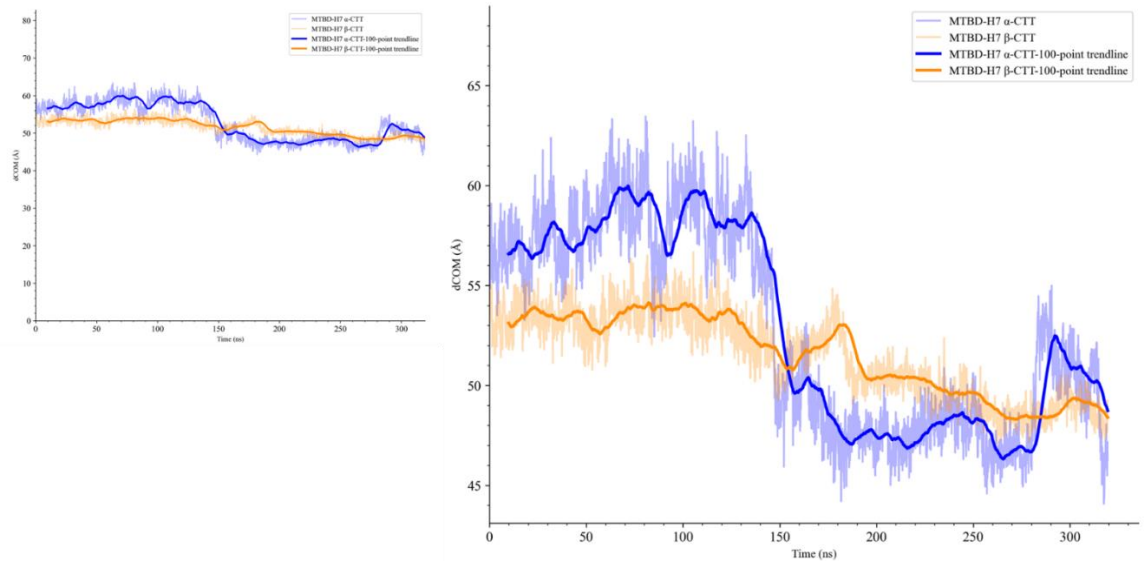


*Note.* The light blue line represents the original dCOM values between α-tubulin CTT and MTBD-H7, while the orange line represents the original dCOM values for β-tubulin CTT and MTBD-H7. The dark blue and dark orange lines represent the 100-data point average trend lines for α-tubulin and β-tubulin, respectively.

*This is only a qualitative comparions otherwise frames prior to convergnace are not analytically worthwhile*

**Figure 19**

*dCOM Analysis Between Tubulin CTTs and MTBD-H3*

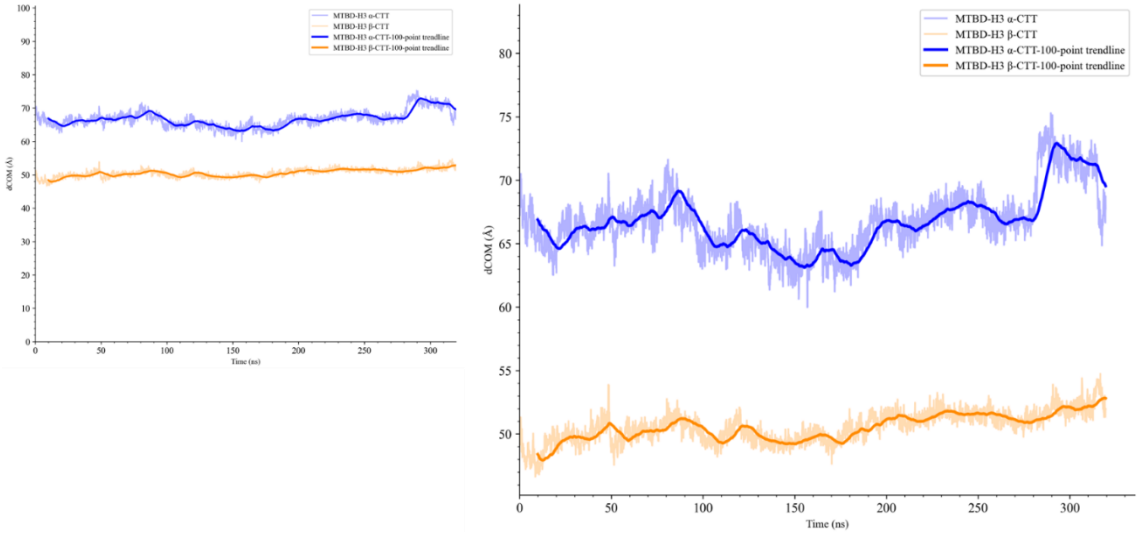


*Note.* The light blue line represents the original dCOM values between α-tubulin CTT and MTBD-H3, while the orange line represents the original dCOM values for β-tubulin CTT and MTBD-H3. The dark blue and dark orange lines represent the 100-data point average trend lines for α-tubulin and β-tubulin, respectively.

*This is only a qualitative comparions otherwise frames prior to convergnace are not analytically worthwhile*

**Figure 20**

d*COM Analysis of Between Tubulin and MTBD-H5*

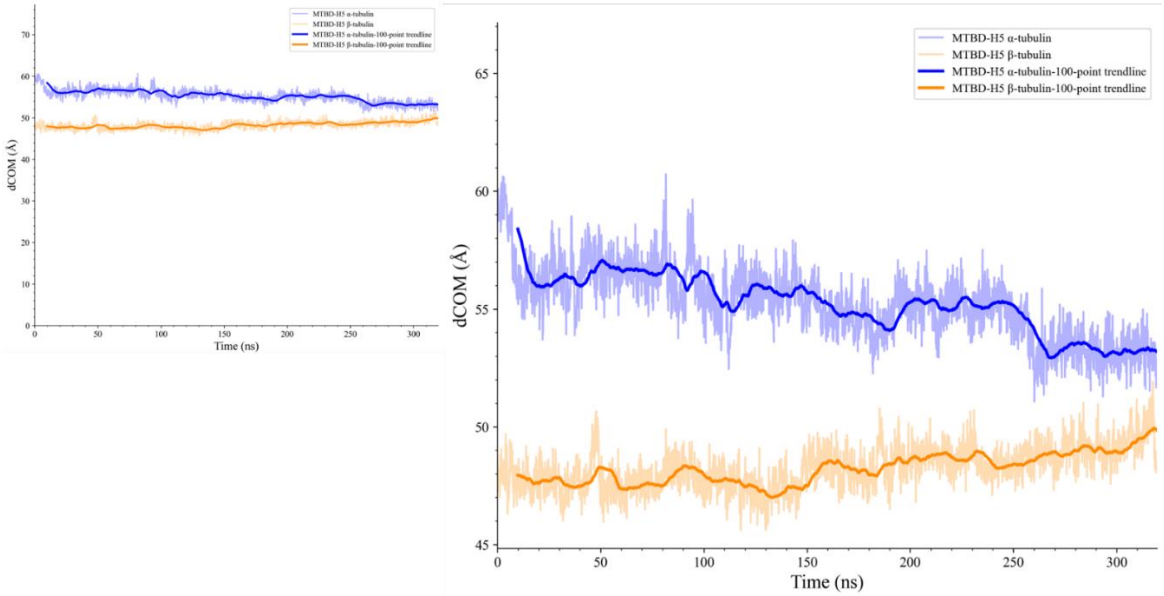


*Note*. The light blue line shows the original dCOM values between α-tubulin and MTBD-H5, while the orange line represents the original dCOM values for β-tubulin and MTBD-H5. The dark blue and dark orange lines represent the 100-data point average trend lines for α-tubulin and β-tubulin, respectively.

*This is only a qualitative comparions otherwise frames prior to convergnace are not analytically worthwhile*

**Figure 21**

d*COM Analysis of Between Tubulin and MTBD-H3*

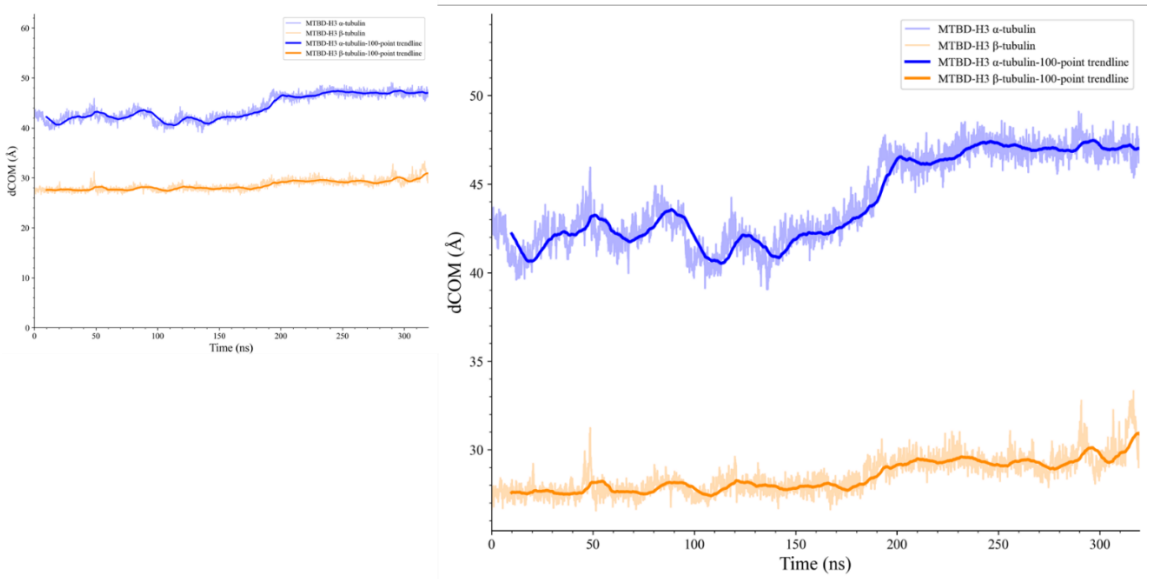


*Note.* The light blue line indicates the original dCOM values between α-tubulin and MTBD-H3, while the orange line represents the original dCOM values for β-tubulin and MTBD-H3. The dark blue and dark orange lines represent the 100-data point average trend lines for α-tubulin and β-tubulin, respectively.

*This is only a qualitative comparions otherwise frames prior to convergnace are not analytically worthwhile*

**Figure 22**

d*COM Analysis of Between Tubulin and MTBD-H1*

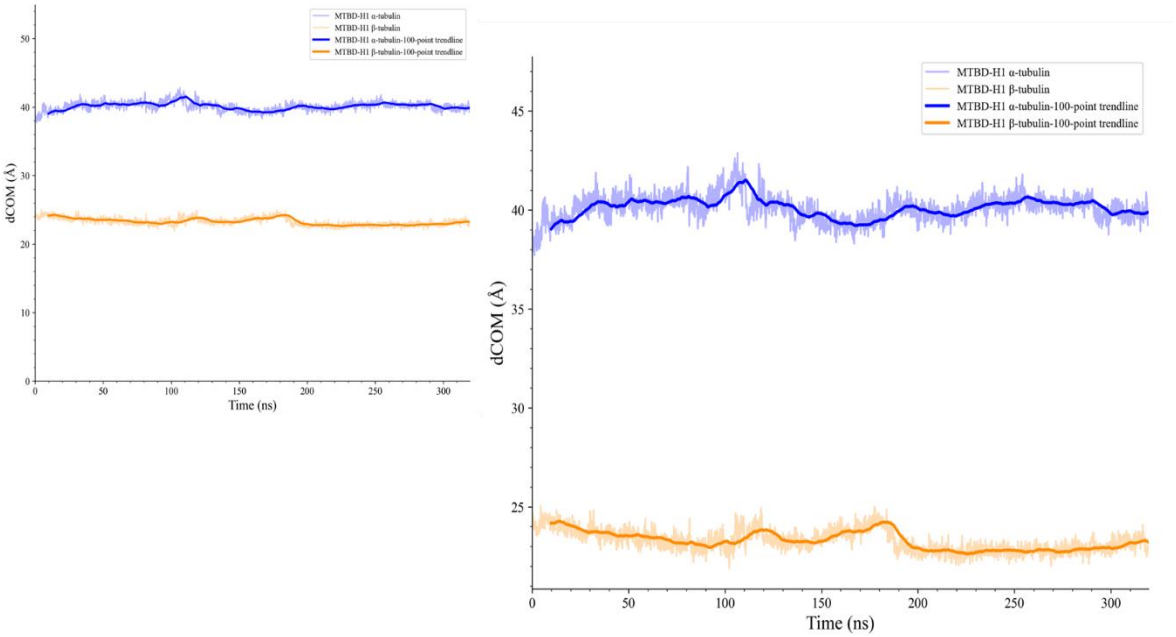


*Note.* The light blue line illustrates the original dCOM values between α-tubulin and MTBD-H1, while the orange line represents the original dCOM values for β-tubulin and MTBD-H1. The dark blue and dark orange lines represent the 100-data point average trend lines for α-tubulin and β-tubulin, respectively.

*This is only a qualitative comparions otherwise frames prior to convergnace are not analytically worthwhile*

### 3.4 Salt Bridge Analysis of System Components

A detailed analysis was conducted to identify potential salt bridge interactions between the MTBD helices (H1-H7) and α- and β-tubulin. A salt bridge was found between the α-H16-H17 loop residue Glu414 and MTBD-H7 residue Arg3384. (Figure 18)

Further salt bridges were identified between α-H17 and MTBD-H7, specifically between residues Glu420, Glu423, Glu417, and Asp424 of α-H17 and Arg3384 of MTBD-H7. A salt bridge was identified between residue GLU414 of β-H18 and ARG3384 of MTBD-H7. Another salt bridge was observed between β-H8 residue GLU194 and ARG3308 of MTBD-H7. In the interaction between β-tubulin and MTBD-H3, a salt bridge was identified between the β-H7 residue GLU158 and the MTBD-H3 residue ARG3339. Another salt bridge was observed between β- residue B4-H7 loop and ARG3339 of MTBD-H3. Finally a salt bridge was discovered between Glu194 on H8 of β-tubulin and Arg3308 on H1 of the MTBD. (Figure18)

**Figure 23**

*Structural Insight into Dynein MTBD-Tubulin Interaction via Salt Bridges*

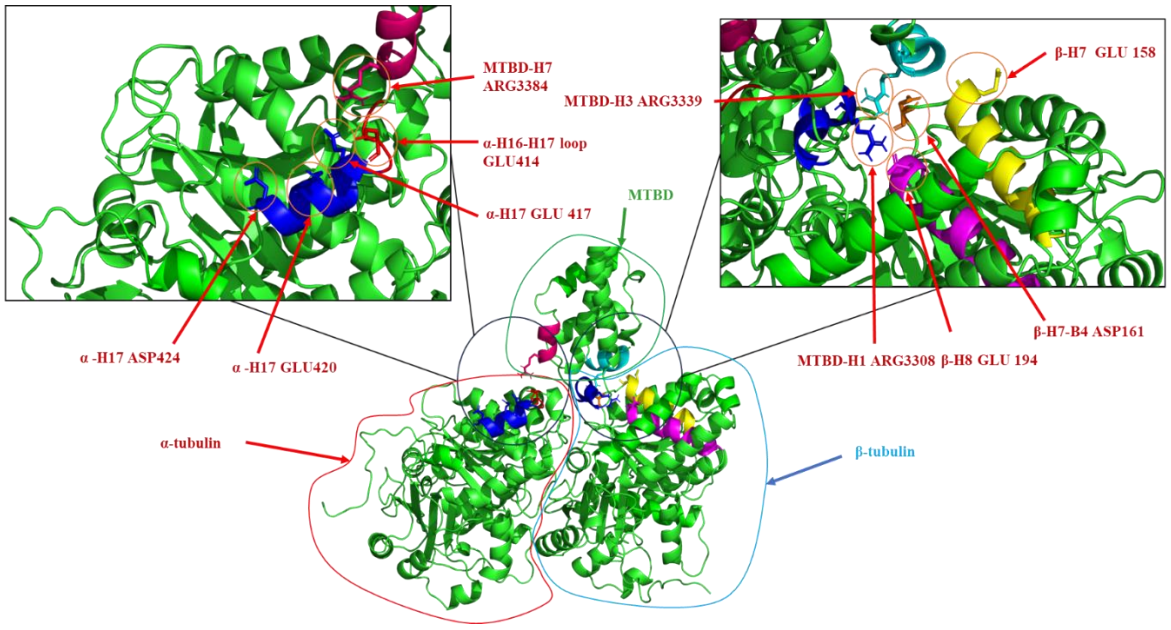


*Note.* The salt bridge interactions between dynein's MTBD and α- and β-tubulin. Within α-tubulin, the α-H17 and associated salt bridge residues are represented (blue). The MTBD-H7 of dynein and its interacting residues are shown (dark pink). In β-tubulin, H8 and its salt bridge residue are portrayed (magenta), the β-H7-B4 loop (orange), and H1 (yellow). Dynein's MTBD-H3 and its corresponding salt bridge residue are illustrated (cyan). Each color-coded highlight represents key amino acids involved in salt bridge formation, essential for the dynein-tubulin interaction.

*This is only a qualitative comparions otherwise frames prior to convergnace are not analytically worthwhile*

# 4. Discussion

## 4.1 RMSD of System Components

RMSD of the complete system displayed large fluctuation in RMSD values, indicating the system is going through significant conformational changes. Upon the removal of the tubulin CTTs and the unbound dynein stalk, the RMSD fluctuations were smaller in comparison to the whole system( Figure8).

The CTTs of tubulins and dynein stalk are unbound regions, contributing to these fluctuations due to it is potential for independent movement, contributing to the high fluctuations in the RMSD of the whole system(i.e including the stalk and CTTs of tubulin, Figure 9)

Although upon removal of the unbound regions α-CTT (Val 437-Tyr451), β-CTT (Gln 426 – Lys 450) and two stalk helices decreased from 7.53 Å to 3.5 Å the fluctuations in the RMSD of the system, the analysis indicated continuous increases, as shown by the 100-point trend line. increases, indicating the system is still going through conformational changes and still hasn't converged (Figure 10).

An RMSD analysis was also done on the components' CTTs individually. Figure The data indicated that the CTTs of the tubulin contribute to overall RMSD of the system, with significant fluctuations in RMSD. The CTTs of tubulins are highly variable regions, which could contribute to the high fluctuations in the RMSD.

Overall, the RMSD analysis findings suggest that the system did not fully converge and that CTTs play a role in the structural stability and the conformational changes as they

fluctuate significantly in the dynein-tubulin complex. However, further analysis is needed to fully understand the implications of these findings.

### 4.2 RMSF of System Components

RMSF analysis is a crucial tool for understanding structural flexibility and stability. In α-tubulin, LYS 338, ARG 339 in the α-H14-B10 loop, and THR 337 in α-H14 displayed significant flexibility with high RMSF values of 9.28 Å, 9.04 Å, and 9.06 Å, respectively. Located near the MT-MTBD interface, these residues could play a critical role in high-affinity MTBD interactions due to their substantial conformational flexibility, possibly resulting from electrostatic attractive or repulsive forces (Figure 14).

A similar pattern emerged from the RMSF analysis of β-tubulin. Residues such as HIS 396 (7.18 Å), GLY 400 (7.15 Å), and GLU 401 (7.38 Å) in β-H17, along with GLY 402 (7.04 Å) in β-H17-H18 loop and LYS 392 (7.16 Å) in β-H16-H17 loop, displayed high RMSF values. Their proximity to the MT-MTBD interface, along with their high flexibility, suggests a potential role in the conformational changes during MTBD binding, influenced by electrostatic forces (Figure 14).

Additional regions in β-tubulin, specifically β-H5 (LYS 103, 7.16 Å and TYR 106, 7.30 Å) and the β–H4-H5 loop (ALA 97, 7.27 Å, ASN 99, 7.20 Å, and GLY 96, 7.17 Å), exhibited high RMSF values. Although not directly adjacent to the MT-MTBD interface, these flexible residues may play an essential role in transmitting conformational changes throughout the system, integral for the high-affinity binding of MTBD and MT interface.

These changes also be a manifestation of electrostatic forces from charged amino acid at work (Figure 14).

The RMSF analysis of the MTBD highlighted high flexibility in MTBD-H7 and MTBD-H3, with residues like GLU 3380 in MTBD-H7 having an RMSF value of 5.97 Å. In contrast, MTBD-H1 and MTBD-H4 showed relative stability, as evidenced by residues like VAL 3305 in MTBD-H1 with an RMSF of 4.59 Å. The dynamic behaviour of these residues suggests that they may contribute to the MTBD's adaptability to different physiological conditions, potentially through modulation by electrostatic forces (Figure 15).

The relative rigidity observed in regions like MTBD-H1 and MTBD-H4 could provide precision to microtubule binding interactions, ensuring the necessary stability for dynein's motor function, which could be influenced by attractive electrostatic forces contributing to high-affinity binding The dynamic behaviour of the residues, indicated by their varying RMSF values, suggests that these elements may contribute to the MTBD's ability to adapt to different physiological conditions. It is important to note, however, that these conclusions are based on the observed data in a non converged short trajectory and thus require a complete MD simulation and more detailed investigations to confirm the implications of these structural dynamics

### 4.3 dCOM Analysis and Potential Interactions between System Components

In previous works, a dCOM analysis has been employed to determine potential interactions between different system components (Heale & Alisaraie., 2020). The dCOM

analysis conducted between α-tubulin and the MTBD indicated that the distance between alpha-tubulin and the MTBD decreased; this indicates that the interaction between MTBD and α-tubulin over the course of the simulation became stronger at the interface of the two domains. In comparison, the distance between β-tubulin and MTBD increased over the course of the simulation, indicating these segments moved farther apart(Figure 16). However, as the system is not converged that observation cannot provide any reliable information.

The dCOM analysis between β-tubulin and MTBD in a convergance system could indicate weaking interactions, when the distance between between β-tubulin and MTBD decreases. The interaction between α-tubulin and the MTBD a strengthening of the interaction, as the distance between α-tubulin and the MTBD decreases.

These observations align with those reported by Heale and Alisaraie (2020). Heale and Alisaraie also reported fluctuating changes in dCOM in the MTBD's interactions with tubulin subunits, reinforcing the dynamic nature of these proteins. Their results demonstrated a similar pattern, with an increased dCOM for β-tubulin and a decrease for α-tubulin.

The decrease in dCOM between the MTBD and α-tubulin components, including its CTT, from 46.5 Å to 44.9 Å and 66.9 Å to 60.5 Å respectively, indicates a strengthening of the interactions (Figure 17). This suggests that α-tubulin and its CTT could be crucial in facilitating a robust interaction with the MTBD, possibly enhancing the MTBD's alignment or attachment to the microtubule.

The interaction between the MTBD and β-tubulin, as well as its CTT, displayed a more modest strengthening, with the dCOM decreasing from 34.5 Å to 34.0 Å and 52.8 Å to 52.0 Å, respectively (Figure 17). In a converged system, such a subtle difference may imply an alternative interaction dynamic within the system, wherein β-tubulin and its CTT might have a nuanced role in maintaining the MTBD binding affnity, a potential variation worth exploring further.

Of particular interest is the significant decrease in dCOM between the MTBD's helix H7 and α-tubulin's CTT, from 56.4 Å to 46.3 Å (Figure. 18). This implies improving interactions over time; and considering the involved amino acids' electrostatic properties, this could play a crucial role in maintaining the stability or enhancing the functionality of dynein's motor mechanism.

On the contrary, an increase in dCOM from 49.9 Å to 52.0 Å was observed between β-tubulin's CTT and the MTBD's helix H3 (Figure 19). This divergence suggests a weakening of the electrostatic interaction or a change in the interaction mode, signifying a potentially different dynamic with an unclear functional impact that calls for more comprehensive studies.

Furthermore, while the interaction between MTBD's helix H5 and α-tubulin led to a notable decrease in dCOM from 77.6 Å to 63.7 Å (Figure 20), signifying stronger electrostatic interaction, the MTBD's helix H3 and β-tubulin interaction conversely showed an increase in dCOM from 49.1 Å to 52.0 Å (Figure 21).

The observed decrease in dCOM from 23.9 Å to 22.8 Å between MTBD-H1 and β-tubulin (Figure 22).which signals a strengthening of interactions and potential enhancement in the MTBD binding affinity that corroborates with previous literature. Both Redwine et al. (2012) and Heale and Alisare (2020) reported similar observations, further substantiating the potential significance of this interaction dynamic within the dynein-tubulin system. This decrease, indicates a repositioning of H1 closer to β-tubulin, coincides with conformational alterations in the CC1 coil. Such movements influence the coiled-coil towards a high-affinity state, potentially augmenting binding interactions between the MTBD and the tubulin. Moreover, this shift towards a high-affinity state propagates to the motor domain of dynein, influencing its motor activity and functional performance.

## 4.4 Salt Bridge Analysis

The salt bridge analysis between MTBD and α- and β-tubulin indicate regulation of dynein binding and emphasize the potential for nuanced, electrostatic interactions between these proteins. Notably, the salt bridges identified between α-tubulin and MTBD-H7 suggest that this helix plays a significant role in the binding of dynein to the microtubule. The multiple salt bridges observed between residues Glu420, Glu423, Glu417, and Asp424 of α-H17 and Arg3384 of MTBD-H7 further emphasize the importance of this interaction (Figure 23).

These findings suggest that the specific interactions between α-tubulin and the MTBD, particularly involving MTBD-H7, could be key determinants of the stability and function of the dynein-microtubule complex. The analysis of salt bridge interactions

between the MTBD and β-tubulin indicates a significant role in the binding of dynein to the microtubule. Notably, several salt bridges were identified between β-tubulin and MTBD-H7 and MTBD-H3, suggesting that these helices are key components in the MTBD-β-tubulin interface. For instance, a salt bridge was identified between Glu414 of β-H18 and Arg3384 of MTBD-H7, and another between Glu194 of β-H8 and Arg3308 of MTBD-H6. In the interaction between β-tubulin and MTBD-H3, a salt bridge was identified between Glu158 of β-H7 and Arg3339 of MTBD-H3. An additional salt bridge was observed between the β-H7 and Arg3339 of MTBD-H3.

Given the discrepancy in helix numbering in various studies, it's important to note that what is referred to as the MTBD-H7 in this research corresponds to the H6 helix as defined in the work of Redwine et al. (2012). Despite the difference in designations, both these helices occupy similar positions within the MTBD structure, thereby underlining the relevance of careful comparative interpretation.

Comparing the current work with that of Redwine et al. (2012), it's clear that both studies show how dynein and tubulin interact. Redwine and colleagues found that a specific part of the MTBD (Lys3298 in H1, *Saccharomyces cerevisiae*) can form salt bridges, with different parts of β-tubulin and the MTBD itself. In the current study with Homo sapien dynein, a similar type of interaction was seen with Arg3384 in MTBD-H7.

Redwine et al. (2012) also found that another part of the MTBD (Arg3382 in H6, *Saccharomyces cerevisiae*) can form salt bridges with different parts of α-tubulin and within the MTBD itself. Similarly, in the current work, it was found that Arg3384 in

MTBD-H7 and Arg3308 in MTBD-H6 behaved similarly, forming salt bridges with parts of β-tubulin.

While the some specifics details differ, both the current study and the work of Redwine et al. (2012) agree that these salt bridge interactions are crucial for dynein's binding to tubulin. Moreover, the current study found that the MTBD-H7 region of dynein, which corresponds to the H6 in Redwine et al. (2012)'s work, plays a significant role in this process.

Redwine et al.(2012) described Lys3298 on H1 of the MTBD forming salt bridges with Glu420 on β-tubulin, and a different scenario where Arg3382 in H6 of the MTBD alternated between forming salt bridges with Glu414 and Glu420 on α-tubulin. The current study mirrors this concept of dynamic salt bridge formation, but identifies a new interaction involving Glu194 on H8 of β-tubulin and Arg3308 on H1 of the MTBD. Heale and Alisaraie (2020) reported a similar mechanism where a salt bridge was detected between Glu3390 (MTBD-H1) and Arg402 (α-H14-H15 loop), among others.

This interaction could potentially influence the conformation and movements of the coiled-coil 1 (CC1) region of the dynein stalk. The CC1 domain plays a crucial role in the regulation of dynein activity and is known to undergo shifts during the ATPase cycle. Given that the Arg3308 residue is part of the H1 helix in the MTBD, which directly interacts with the CC1 domain, it's possible that the formation and disruption of the salt bridge with β-tubulin could cause or contribute to these shifts in the CC1. Moreover, since dynein's movement along the microtubule is essentially powered by these ATP-driven

conformational changes, this salt bridge may also have implications for dynein motility. By potentially affecting the ATPase activity and hence the conformational dynamics of the dynein molecule, it could influence the stepping pattern of dynein along the microtubule, and thus, the overall motility of dynein.

Overall the fact that these various salt bridge interactions are seen in different organisms suggests that these are not random occurrences. Instead, they indicate an evolutionarily conserved mechanism contributing to the function of dynein and its interaction with tubulin. These findings highlight the complexity of these interactions and demonstrate the need for further research to fully understand this crucial cellular process

## 5. Conclusion

In conclusion, the comprehensive analysis of the dynein-tubulin system, including the MTBD and CTTs of α- and β-tubulin, has provided some level of insights into the dynamic behaviour and potential interactions within this complex. RMSD analysis revealed significant conformational changes and suggested that the CTTs and the dynein stalk contribute significantly to the dynamics of the system.

The dCOM analysis indicated potential interactions between the CTTs and the MTBD. There was a notable decrease in the dCOM between the MTBD and the C-terminal tail of α-tubulin. In comparison, the salt bridge analysis revealed potential electrostatic interactions, particularly involving the H1, H7 and H3 helices of MTBD and tubulin dimer. Interestingly, no conventional salt bridges between the CTTs and the MTBD, hinting at an unconventional interaction scenario.

Overall, analysis of the complete trajectory could provide a general understanding the dynein-tubulin system's dynamic behaviour and highlight the importance of the CTTs and the dynein stalk in these dynamics. They open up new avenues for research into the function of dynein and the development of dynein-targeted therapies. Further analysis and extended simulation time are required to confirm the quliative analysis presented here based on a small data set obtainable during the limited time of my honours program. A complete study is required to fully understand their implications.

## 6. References

Abraham, M., Alekseenko, A., Bergh, C., Blau, C., Briand, E., Doijade, M., Fleischmann, S., Gapsys, V., Garg, G., Gorelov, S., Gouaillardet, G., Gray, A., Irrgang, M. E., Jalalypour, F., Jordan, J., Junghans, C., Kanduri, P., Keller, S., Kutzner, C., Lindahl, E. (2023). *GROMACS 2023 Manual*. https://doi.org/10.5281/zenodo.7588711.

Aiken, J., Moore, J. K., & Bates, E. A. (2019). TUBA1A mutations identified in lissencephaly patients dominantly disrupt neuronal migration and impair dynein activity. *Human Molecular Genetics*, *28*(8), 1227–1243. https://doi.org/10.1093/hmg/ddy416.

Alushin, G. M., Lander, G. C., Kellogg, E. H., Zhang, R., Baker, D., & Nogales, E. (2014). High-resolution microtubule structures reveal the structural transitions in αβ-tubulin upon GTP hydrolysis. *Cell*, *157*(5), 1117–1129. https://doi.org/10.1016/j.cell.2014.03.053.

Ayloo, S., Guedes-Dias, P., Ghiretti, A. E., & Holzbaur, E. L. F. (2017). Dynein efficiently navigates the dendritic cytoskeleton to drive the retrograde trafficking of BDNF/TrkB signalling endosomes. *Molecular Biology of the Cell*, *28*(19), 2543–2554. https://doi.org/10.1091/mbc.e17-01-0068.

Ban, X., Lahiri, P., Dhoble, A. S., Li, D., Gu, Z., Li, C., Cheng, L., Hong, Y., Li, Z., & Kaustubh, B. (2019). Evolutionary Stability of Salt Bridges Hints It is Contribution to Stability of Proteins. *Computational and Structural Biotechnology Journal*, *17*, 895–903. https://doi.org/10.1016/j.csbj.2019.06.022.

Bodakuntla, S., Yuan, X., Genova, M., Gadadhar, S., Leboucher, S., Birling, M.-C., Klein, D., Martini, R., Janke, C., & Magiera, M. M. (2021). Distinct roles of α- and β-tubulin polyglutamylation in controlling axonal transport and in neurodegeneration. The EMBO Journal, 40(17), e108498. https://doi.org/10.15252/embj.2021108498

Burgess, S. A., Walker, M. L., Sakakibara, H., Knight, P. J., & Oiwa, K. (2003). Dynein structure and power stroke. *Nature*, *421*(6924), 715-718. https://doi.org/10.1038/nature01377.

Burgess, S. A., Walker, M. L., Sakakibara, H., Oiwa, K., & Knight, P. J. (2004). The structure of dynein-c by negative stain electron microscopy. *Journal of Structural Biology*, *146*(1–2), 205–216. https://doi.org/10.1016/j.jsb.2003.10.005.

Bussi, G., Donadio, D., & Parrinello, M. (2007). Canonical sampling through velocity rescaling. *The Journal of Chemical Physics*, *126*(1), Article 014101. https://doi.org/10.1063/1.2408420

Carter, A. P. (2013). Crystal clear insights into how the dynein motor moves. *Journal of Cell Science*, *126*(Pt 3), 705–713. https://doi.org/10.1242/jcs.120725.

Chakraborti, S., Natarajan, K., Curiel, J., Janke, C., & Liu, J. (2016). The emerging role of the tubulin code: From the tubulin molecule to neuronal function and disease. *Cytoskeleton*, *73*(10), 521–550. https://doi.org/10.1002/cm.21290.

Chen, X.-J., Xu, H., Cooper, H. M., & Liu, Y. (2014). Cytoplasmic dynein: A key player in neurodegenerative and neurodevelopmental diseases. *Science China Life Sciences*, *57*(4), 372–377. https://doi.org/10.1007/s11427-014-4639-9.

Cho, C., Reck-Peterson, S. L., & Vale, R. D. (2008). Regulatory ATPase sites of cytoplasmic dynein affect processivity and force generation. *The Journal of Biological Chemistry*, *283*(38), 25839–25845. https://doi.org/10.1074/jbc.M802951200.

DeWitt, M. A., Cypranowska, C. A., Cleary, F. B., Belyy, V., & Yildiz, A. (2015). The AAA3 domain of cytoplasmic dynein acts as a switch to facilitate microtubule release. *Nature Structural & Molecular Biology*, *22*(1), 73-80. https://doi.org/10.1038/nsmb.2930.

Dodda, L. S., Cabeza de Vaca, I., Tirado-Rives, J., & Jorgensen, W. L. (2017). LigParGen web server: An automatic OPLS-AA parameter generator for organic ligands. *Nucleic Acids Research*, *45*(W1), W331–W336. https://doi.org/10.1093/nar/gkx312.

Dutta, M., & Jana, B. (2019). Role of AAA3 Domain in Allosteric Communication of Dynein Motor Proteins. *ACS Omega*, *4*(26), 21921–21930. https://doi.org/10.1021/acsomega.9b02946.

Dutta, M., & Jana, B. (2021). Computational modelling of dynein motor proteins at work. *Chemical Communications*, *57*(3), 272–283. https://doi.org/10.1039/D0CC05857B

Essmann, U., Perera, L., Berkowitz, M. L., Darden, T., Lee, H., & Pedersen, L. G. (1995). A smooth particle mesh Ewald method. *The Journal of Chemical Physics*, *103*(19), 8577–8593. https://doi.org/10.1063/1.470117.

Ferro, L. S., Eshun-Wilson, L., Gölcük, M., Fernandes, J., Huijben, T., Gerber, E., Jack, A., Costa, K., Gür, M., Fang, Q., Nogales, E., & Yildiz, A. (2020). *The mechanism of*

*motor inhibition by microtubule-associated proteins* (p. 2020.10.22.351346). bioRxiv. https://doi.org/10.1101/2020.10.22.351346.

Gardner, M. K. (2016). Cell Biology: Microtubule Collisions to the Rescue. *Current Biology*, *26*(24), R1287–R1289. https://doi.org/10.1016/j.cub.2016.11.010

Gardner, M. K., Zanic, M., & Howard, J. (2013). Microtubule catastrophe and rescue. *Current Opinion in Cell Biology*, *25*(1), 14–22. https://doi.org/10.1016/j.ceb.2012.09.006.

Gibbons, I. R. (1981). Cilia and flagella of eukaryotes. *The Journal of Cell Biology*, *91*(3), 107-124. https://doi.org/10.1083/jcb.91.3.107s.

Gowers, R., Linke, M., Barnoud, J., Reddy, T., Melo, M., Seyler, S., Domański, J., Dotson, D., Buchoux, S., Kenney, I., & Beckstein, O. (2016). MDAnalysis: A Python Package for the Rapid Analysis of Molecular Dynamics Simulations. 98–105. https://doi.org/10.25080/Majora-629e541a-00e.

Goodson, H. V., & Jonasson, E. M. (2018). Microtubules and Microtubule-Associated Proteins. *Cold Spring Harbor Perspectives in Biology*, *10*(6). Article #? https://doi.org/10.1101/cshperspect.a022608.

Guvench, O., & MacKerell, A. D. (2008). Comparison of Protein Force Fields for Molecular Dynamics Simulations. In A. Kukol (Ed.), *Molecular Modeling of Proteins* (pp. 63–88). Humana Press. https://doi.org/10.1007/978-1-59745-177-2_4.

Heale, K. A., & Alisaraie, L. (2020). C-terminal Tail of β-Tubulin and it is Role in the Alterations of Dynein Binding Mode. *Cell Biochemistry and Biophysics*, *78*(3), 331–345. https://doi.org/10.1007/s12013-020-00920-7.

Hess, B., Bekker, H., Berendsen, H. J. C., & Fraaije, J. G. E. M. (1997). LINCS: A linear constraint solver for molecular simulations. *Journal of Computational Chemistry*, *18*(12), 1463–1472. https://doi.org/10.1002/(SICI)1096-987X(199709)18:12<1463::AID-JCC4>3.0.CO;2-H.

Humphrey, W., Dalke, A., & Schulten, K. (1996). VMD: Visual molecular dynamics. Journal of Molecular Graphics, 14(1), 33–38, 27–28. https://doi.org/10.1016/0263-7855(96)00018-5

Howard, J. (1997). Molecular motors: Structural adaptations to cellular functions. *Nature*, *389*(6651), 561-567. https://doi.org/10.1038/39247.

Janke, C., & Magiera, M. M. (2020). The tubulin code and it is role in controlling microtubule properties and functions. *Nature Reviews Molecular Cell Biology*, *21*(6), 307-326. https://doi.org/10.1038/s41580-020-0214-3.

Karki, S., & Holzbaur, E. (1999). Cytoplasmic dynein and dynactin in cell division and intracellular transport. *Current Opinion in Cell Biology*, *11*(1), 45-53. https://doi.org/10.1016/s0955-0674(99)80006-4.

Kimura, N., & Yanagisawa, K. (2018). Traffic jam hypothesis: Relationship between endocytic dysfunction and Alzheimer's disease. *Neurochemistry International*, *119*, 35–41. https://doi.org/10.1016/j.neuint.2017.07.002.

Kon, T., Oyama, T., Shimo-Kon, R., Imamula, K., Shima, T., Sutoh, K., & Kurisu, G. (2012). The 2.8 Å crystal structure of the dynein motor domain. *Nature*, *484*(7394), 345–350. https://doi.org/10.1038/nature10955.

Kowiański, P., Lietzau, G., Czuba, E., Waśkow, M., Steliga, A., & Moryś, J. (2018). BDNF: A Key Factor with Multipotent Impact on Brain Signaling and Synaptic Plasticity. *Cellular and Molecular Neurobiology*, *38*(3), 579–593. https://doi.org/10.1007/s10571-017-0510-4.

Knapp, B., Frantal, S., Cibena, M., Schreiner, W., & Bauer, P. (2011). Is an Intuitive Convergence Definition of Molecular Dynamics Simulations Solely Based on the Root Mean Square Deviation Possible? Journal of Computational Biology, 18(8), 997–1005. https://doi.org/10.1089/cmb.2010.0237.

Kumar, S., & Nussinov, R. (2002). Close-Range Electrostatic Interactions in Proteins. ChemBioChem,3(7),604-617. https://doi.org/10.1002/14397633(20020703)3:7<604::AID-CBIC604>3.0.CO;2-X.

LaMonte, B. H., Wallace, K. E., Holloway, B. A., Shelly, S. S., Ascaño, J., Tokito, M., Van Winkle, T., Howland, D. S., & Holzbaur, E. L. F. (2002). Disruption of Dynein/Dynactin Inhibit is Axonal Transport in Motor Neurons Causing Late-Onset Progressive Degeneration. *Neuron*, *34*(5), 715–727. https://doi.org/10.1016/S0896-6273(02)00696-7.

Leach, A. R., & AR, L. (2001). *Molecular Modelling: Principles and Applications*. Prentice Hall.

Lin, J., Okada, K., Raytchev, M., Smith, M. C., & Nicastro, D. (2014). Structural mechanism of the dynein power stroke. *Nature Cell Biology*, *16*(5), 479–485. https://doi.org/10.1038/ncb2939.

Manna, R. N., Dutta, M., & Jana, B. (2020). Mechanistic study of the ATP hydrolysis reaction in dynein motor protein. *Physical Chemistry Chemical Physics*, *22*(3), 1534–1542. https://doi.org/10.1039/C9CP02194A.

Marinković, P., Reuter, M. S., Brill, M. S., Godinho, L., Kerschensteiner, M., & Misgeld, T. (2012). Axonal transport deficit is and degeneration can evolve independently in mouse models of amyotrophic lateral sclerosis. *Proceedings of the National Academy of Sciences of the United States of America*, *109*(11), 4296–4301. https://doi.org/10.1073/pnas.1200658109.

Martínez, L. (2015). Automatic Identification of Mobile and Rigid Substructures in Molecular Dynamics Simulations and Fractional Structural Fluctuation Analysis. PLOS ONE, 10(3), e0119264. https://doi.org/10.1371/journal.pone.0119264.

Markus, S. M., Marzo, M. G., & McKenney, R. J. (2020). New insights into the mechanism of dynein motor regulation by lissencephaly-1. *ELife*, *9*, Article e59737. https://doi.org/10.7554/eLife.59737.

Metropolis, N., Rosenbluth, A. W., Rosenbluth, M. N., Teller, A. H., & Teller, E. (2004). Equation of State Calculations by Fast Computing Machines. *The Journal of Chemical Physics*, *21*(6), 1087–1092. https://doi.org/10.1063/1.1699114.

Michaud-Agrawal, N., Denning, E. J., Woolf, T. B., & Beckstein, O. (2011). MDAnalysis: A toolkit for the analysis of molecular dynamics simulations. Journal of Computational Chemistry, 32(10), 2319–2327. https://doi.org/10.1002/jcc.21787.

Millecamps, S., & Julien, J.-P. (2013). Axonal transport deficit is and neurodegenerative diseases. *Nature Reviews. Neuroscience*, *14*(3), 161–176. https://doi.org/10.1038/nrn3380.

Moughamian, A. J., & Holzbaur, E. L. F. (2018). 13—Cytoplasmic dynein dysfunction and neurodegenerative disease. In S. M. King (Ed.), *Dyneins: Structure, Biology and Disease (Second Edition)* (pp. 286–315). Academic Press. https://doi.org/10.1016/B978-0-12-809470-9.00013-8.

Paschal, B. M., & Vallee, R. B. (1987). Retrograde transport by the microtubule-associated protein MAP 1C. *Nature*, *330*(6144), 181-183. https://doi.org/10.1038/330181a0.

Perlson, E., Jeong, G.-B., Ross, J. L., Dixit, R., Wallace, K. E., Kalb, R. G., & Holzbaur, E. L. F. (2009). A switch in retrograde signaling from survival to stress in rapid-onset neurodegeneration. *The Journal of Neuroscience*, *29*(31), 9903–9917. https://doi.org/10.1523/JNEUROSCI.0813-09.2009.

Pfister, K. K., Fisher, E. M. C., Gibbons, I. R., Hays, T. S., Holzbaur, E. L. F., McIntosh, J. R., Porter, M. E., Schroer, T. A., Vaughan, K. T., Witman, G. B., King, S. M., & Vallee, R. B. (2005). Cytoplasmic dynein nomenclature. *Journal of Cell Biology*, *171*(3), 411–413. https://doi.org/10.1083/jcb.200508078.

Prahlad, V., Helfand, B. T., Langford, G. M., Vale, R. D., & Goldman, R. D. (2000). Fast transport of neurofilament protein along microtubules in squid axoplasm. *Journal of Cell Science*, *113*(22), 3939–3946. https://doi.org/10.1242/jcs.113.22.3939.

Ramkumar, A., Jong, B. Y., & Ori-McKenney, K. M. (2018). ReMAPping the microtubule landscape: How phosphorylation dictates the activities of microtubule-associated proteins. Developmental Dynamics, 247(1), 138–155. https://doi.org/10.1002/dvdy.24599.

Ravikumar, B., Acevedo-Arozena, A., Imarisio, S., Berger, Z., Vacher, C., O'Kane, C. J., Brown, S. D. M., & Rubinsztein, D. C. (2005). Dynein mutations impair autophagic clearance of aggregate-prone proteins. *Nature Genetics*, *37*(7), 771-776. https://doi.org/10.1038/ng1591.

Reck-Peterson, S. L., Redwine, W. B., Vale, R. D., & Carter, A. P. (2018). The cytoplasmic dynein transport machinery and it is many cargoes. *Nature Reviews Molecular Cell Biology*, *19*(6), 382-398. https://doi.org/10.1038/s41580-018-0004-3.

Redwine, W. B., Hernández-López, R., Zou, S., Huang, J., Reck-Peterson, S. L., & Leschziner, A. E. (2012). Structural Basis for Microtubule Binding and Release by Dynein. Science, 337(6101), 1532–1536. https://doi.org/10.1126/science.1224151.

Roberts, A. J., Kon, T., Knight, P. J., Sutoh, K., & Burgess, S. A. (2013). Functions and mechanics of dynein motor proteins. *Nature Reviews. Molecular Cell Biology*, *14*(11), 713–726. https://doi.org/10.1038/nrm3667.

Roberts, A. J., Numata, N., Walker, M. L., Kato, Y. S., Malkova, B., Kon, T., Ohkura, R., Arisaka, F., Knight, P. J., Sutoh, K., & Burgess, S. A. (2009). AAA+ Ring and

Linker Swing Mechanism in the Dynein Motor. *Cell*, *136*(3), 485–495. https://doi.org/10.1016/j.cell.2008.11.049.

Sargsyan, K., Grauffel, C., & Lim, C. (2017). How Molecular Size Impacts RMSD Applications in Molecular Dynamics Simulations. Journal of Chemical Theory and Computation, 13(4), 1518–1524. https://doi.org/10.1021/acs.jctc.7b00028.

Schmid, N., Eichenberger, A. P., Choutko, A., Riniker, S., Winger, M., Mark, A. E., & van Gunsteren, W. F. (2011). Definition and testing of the GROMOS force-field versions 54A7 and 54B7. *European Biophysics Journal*, *40*(7), 843–856. https://doi.org/10.1007/s00249-011-0700-9.

Schrödinger, LLC. (2015). The PyMOL Molecular Graphics System, Version 1.8.

Schuler, L. D., Daura, X., & van Gunsteren, W. F. (2001). An improved GROMOS96 force field for aliphatic hydrocarbons in the condensed phase. *Journal of Computational Chemistry*, *22*(11), 1205–1218. https://doi.org/10.1002/jcc.1078.

Skiniotis, G., Cochran, J. C., Müller, J., Mandelkow, E., Gilbert, S. P., & Hoenger, A. (2004). Modulation of kinesin binding by the C-termini of tubulin. The EMBO Journal, 23(5), 989–999. https://doi.org/10.1038/sj.emboj.7600118

Spiliotis, E. T. (2010). Regulation of microtubule organization and functions by septin GTPases. Cytoskeleton, 67(6), 339–345. https://doi.org/10.1002/cm.20448

Trokter, M., Mücke, N., & Surrey, T. (2012). Reconstitution of the human cytoplasmic dynein complex. *Proceedings of the National Academy of Sciences*, *109*(51), 20895–20900. https://doi.org/10.1073/pnas.1210573110.

Uchimura, S., Fujii, T., Takazaki, H., Ayukawa, R., Nishikawa, Y., Minoura, I., Hachikubo, Y., Kurisu, G., Sutoh, K., Kon, T., Namba, K., & Muto, E. (2015). A flipped ion pair at the dynein–microtubule interface is critical for dynein motility and ATPase activation. *Journal of Cell Biology*, *208*(2), 211–222. https://doi.org/10.1083/jcb.201407039.

Vale, R. D. (2003). The Molecular Motor Toolbox for Intracellular Transport. *Cell*, *112*(4), 467–480. https://doi.org/10.1016/S0092-8674(03)00111-9.

Vale, R. D., Reese, T. S., & Sheetz, M. P. (1985). Identification of a novel force-generating protein, kinesin, involved in microtubule-based motility. *Cell*, *42*(1), 39–50. https://doi.org/10.1016/s0092-8674(85)80099-4.

Vallee, R. B. (2018). 2—Origins of cytoplasmic dynein. In S. M. King (Ed.), *Dyneins: Structure, Biology and Disease (Second Edition)* (pp. 88–99). Academic Press. https://doi.org/10.1016/B978-0-12-809471-6.00002-4.

Vanommeslaeghe, K., Hatcher, E., Acharya, C., Kundu, S., Zhong, S., Shim, J., Darian, E., Guvench, O., Lopes, P., Vorobyov, I., & Mackerell Jr., A. D. (2010). CHARMM general force field: A force field for drug-like molecules compatible with the CHARMM all-atom additive biological force fields. *Journal of Computational Chemistry*, *31*(4), 671–690. https://doi.org/10.1002/jcc.21367.

Vemu, A., Atherton, J., Spector, J. O., Szyk, A., Moores, C. A., & Roll-Mecak, A. (2016). Structure and Dynamics of Single-isoform Recombinant Neuronal Human Tubulin. *The Journal of Biological Chemistry*, *291*(25), 12907–12915. https://doi.org/10.1074/jbc.C116.731133.

Verhey, K. J., & Gaertig, J. (2007). The Tubulin Code. *Cell Cycle*, *6*(17), 2152–2160. https://doi.org/10.4161/cc.6.17.4633.

Weiner, S. J., Kollman, P. A., Nguyen, D. T., & Case, D. A. (1986). An all atom force field for simulations of proteins and nucleic acids. *Journal of Computational Chemistry*, *7*(2), 230–252. https://doi.org/10.1002/jcc.540070216.

Wynshaw-Boris, A. (2007). Lissencephaly and LIS1: Insights into the molecular mechanisms of neuronal migration and development. *Clinical Genetics*, *72*(4), 296–304. https://doi.org/10.1111/j.1399-0004.2007.00888.x.